Remote Sensing Applications: Society and Environment 25 (2022) 100679

Contents lists available at ScienceDirect

Remote Sensing Applications: Society and Environment

journal homepage: www.elsevier.com/locate/rsase

Identification of species of the genus *Acer* L. using vegetation indices calculated from the hyperspectral images of leaves

Pavel A. Dmitriev [a], Boris L. Kozlovsky [a], Denis P. Kupriushkin [a], Vladimir S. Lysenko [a], Vishnu D. Rajput [a], Maria A. Ignatova [a], Ekaterina P. Tarik [a], Olga A. Kapralova [a], Valeriy K. Tokhtar [b], Anil Kumar Singh [c], Tatiana Minkina [a], Tatiana V. Varduni [a], Meenakshi Sharma [d], Ajay Kumar Taloor [e,*], Asha Thapliyal [f]

[a] *Southern Federal University, Rostov-on-Don, Russia*
[b] *Belgorod State University, Belgorod, Russia*
[c] *Department of Earth & Planetary Sciences, University of Allahabad, Prayagraj, 211 002, India*
[d] *Padam Shri Padma Sachdev Government Post Graduate College for Women Gandhi Nagar Jammu, 180003, India*
[e] *Departemnt of Remote Sensing and GIS, University of Jammu,Jammu, 180006 India*
[f] *Uttarakhand Space Application Centre (USAC) Government of Uttarakhand, India*

ARTICLE INFO

Keywords:
Maple
Remote sensing
Cubert UHD-185
Species identification
NDVI

ABSTRACT

Selection of the most suitable spectral vegetation indices which are applicable to the remote sensing of the forest species composition and status, is an important task aimed at the evaluation of the large-scale plant communities. There are 80 vegetation indices have been collected in the present work using the hyperspectral data, including that for the *Acer platanoides* L., *A. saccharinum* L. and *A. pseudoplatanus* L. The obtained data showed that 40 vegetation indices were significantly differed between species in their values simultaneously (all over the experiment) in all the following pairs: *A. saccharinum* – *A. platanoides, A. saccharinum* – *A. pseudoplatanus* and *A. platanoides* – *A. pseudoplatanus. A. platanoides* – *A. pseudoplatanus*: Boochs2, MCARI2, TCARI2, Vogelmann2 and Vogelmann4; *A. platanoides* – *A. saccharinum*: Carter2, Carter3, Carter4, Carter5, CI, CI2, CRI3, CRI4, Datt, Datt2, Datt3, Datt5, DDn, DWSI4, EGFN, EGFR, EVI, GI, GMI1, GMI2, Green NDVI, Maccioni, MCARI2, mSR2, MTCI, NDVI2, NDVI3, OSAVI2, PARS, PSSR, REP_Li, SR1, SR2, SR3, SR4, SR8, Vogelmann2 and Vogelmann4; *A. pseudoplatanus* – *A. saccharinum*: Carter3, Carter5, CRI3, Datt5, Datt6, DWSI4, EGFN, EGFR, GI, GMI1, Green NDVI, NDVI3, PARS, SR3, SR4, SR5, SR8 and TGI. The selected list of the vegetation indices may be recommended for the identification of the maple species using the method of the remote hyperspectral sensing.

1. Introduction

Vegetation cover is a key component for understanding the terrestrial ecosystems (Houborg et al., 2015). Remote hyperspectral sensing provides an powerful tool in researches of the vegetation patterns, including that related to the vegetation types, changes in growth characteristics, physiology, and morphology (Xue and Su, 2017). It is an art combined with science and information technology that helps monitor and manage crop health, soil architecture, weather forecast, temperature, humidity, etc, in real-time (Singh et al.,

* Corresponding author.
E-mail address: ajaytaloor@gmail.com (A.K. Taloor).

https://doi.org/10.1016/j.rsase.2021.100679
Received 25 August 2021; Received in revised form 2 December 2021; Accepted 8 December 2021
Available online 6 January 2022

2020). Hyperspectral imaging implies conducting an analysis of the sunlight or the artificial light reflected from plant leaves using a large number of the spectral bands that increases accuracy, flexibility, quantity and quality of the information obtaining on the vegetation cover. Application of the hyperspectral technique in the ecological monitoring depends on five components. The first of them is choice an ideal energy source or illumination which provides electromagnetic radiation to target objects; second atmosphere and radiation: when sunlight travels to the earth's surface, it comes in contact with the atmosphere and reacts as energy in the form of radiation, the same thing happens with light reflectance; further, third component is interaction of radiation with the target and recording of the reflected energy; fourth component is transmission and ground-level processing. The fourth component comes in picture after the energy perceived has to be transmitted in the form of an electronic signal. Whereas, fifth and last component is interpretation, analysis, and application of data that is detected by ground station through various sensors (Fig. 1). The energy/radiations recorded by ground stations is generally processed and generate the output as an image.

Development of the hyperspectral imaging methods is necessary for the phenotyping analysis and classification of plants, monitoring the soil properties, detecting the crop diseases, estimating crop properties, classifying weeds, mapping crop area, investigating vegetation properties which help in various type of stresses like biotic and abiotic related studies in plants. Plant leaves contain the thin layer of cells that form the leaf's top surface, known as the epidermis. Under the epidermis, two layers of cells are present. Palisade parenchyma cells are on the top and are arranged vertically; this layer contains the photosynthetic pigment chlorophyll that captures the solar energy during photosynthesis. The second lower layer is the spongy parenchyma that has irregularly shaped cells with many air spaces that allow circulation of gases and play an important role in gaseous exchange. Plant palisade parenchyma cells also contain pigments other than chlorophyll for example carotenoids, anthocyanins that absorb almost all the visible electromagnetic energy, especially in the blue and red regions (Wolf and Wolf, 1955). Green light is not absorbed by a leaf, hence vegetation appears green to our eyes. On the other hand, NIR (Near-infrared) is not absorbed by the pigment system of leaf cells resulting in approximately total energy exiting from the lower and top epidermis of the leaf towards the sky (Wu et al., 2014) (Fig. 2). When the plant becomes dehydrated, sick, afflicted with disease, etc., the spongy layer deteriorates, and the plant absorbs more of the near-infrared light, rather than reflecting it.

Thus, observations of how NIR changes in comparision to red light, provides an accurate indication of the presence of chlorophyll, which correlates with plant health (Akhtman et al., 2017). These observations also provide classification of tree plants with the help of hyperspectral imaging platforms and sensors (Fricker et al., 2019). Hyperspectral sensors are connected with different platforms like airplanes, UAVs, satellites, and close-range platforms to capture high resolutions images. Hyperspectral imaging platforms and sensors are categorized into 4 groups 1) Satellite-Based Hyperspectral Imaging 2) Airplane-Based Hyperspectral Imaging 3) UAV-Based Hyperspectral Imaging and 4) Close-Range (Ground- or Lab-Based) Hyperspectral imaging (Table 1) (Lu et al., 2020).

Satellite-based hyperspectral imaging methods have broad perspectives for studying the qualitative and quantitative characteristics of massive woodlands. Today, there is a wide variety of hyperspectral imaging systems that provide spectral or three-dimensional information. In the past 40 years, attempts to identify the species of woody plant samples using hyperspectral imaging methods has increased steadily (Fassnacht et al., 2016). It happened due to the increasing availability of multispectral cameras, due to decrease in their cost as well as due to decrease in their size and weight. Development of unmanned vehicles, and fundamentally new cameras are the other promising tools that add to the purpose (Fassnacht et al., 2014). Unmanned aerial vehicles (UAVs) are well adapted and flexible platforms for cameras these days.

Different approaches and technologies along with different types and combinations of sensors (SAR, LiDAR, and others), cameras (multispectral, hyperspectral, and infrared) have been used for the identification of tree species (Fricker et al., 2019; Hycza et al., 2018; Mäyrä et al., 2021). However, many queries regarding the reliability of existing approaches to the tree species classification remain unanswered (Fassnacht et al., 2014). Large-scale tree species recognition remains a fundamental problem when conducting an inventory of green spaces (Hycza et al., 2018). Studies demonstrate the combination of GPS-based field surveys and drone-operated hyperspectral aerial photography can be used effectively to accurately map the infected areas (Adão et al., 2017). Hyperspectral imaging is an advanced technique and is capable of acquiring a detailed spectral response of target features. Data obtained using hyperspectral sensors provide near continuous spectral reflectance curves. Signatures drawn using these spectral reflectance curves are unique spectral signatures, that enables the calculation of narrow band vegetation indices and consequently, better separation of plant species from each other (Lu et al., 2020). For this report we have selected *Acer* L. genus for remote sensing based vegetation study. The

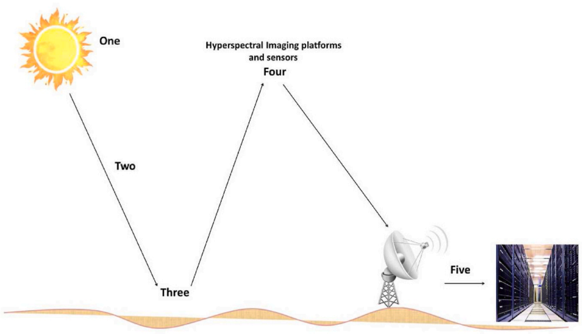

Fig. 1. Diagrammatic representation of hyperspectral Imaging platforms and sensors-based monitoring.

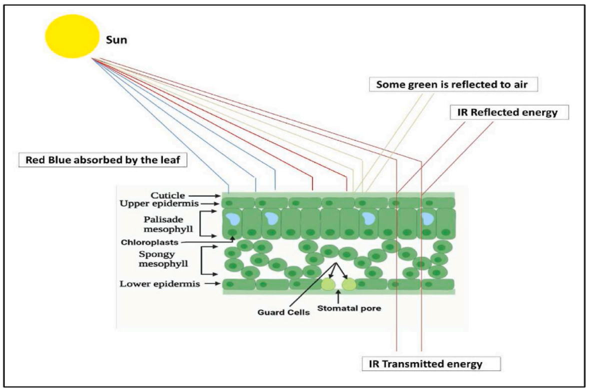

Fig. 2. Cellular leaf structure and its interaction with electromagnetic energy. Mostly visible light is absorbed, while almost half of the near-infrared energy is reflected. These reflections are detected with the help of various hyperspectral imaging platforms and sensors.

Table 1
Hyperspectral imaging sensors and their applications along with imaging platforms.

S. NO	Hyperspectral Imaging platforms	Hyperspectral Imaging sensors (number of spectral channels; spectral range, nm)	Application	Reference
1.	Satellite-Based Hyperspectral Imaging	Hyperion (220; 430–2400), PROBA-CHRIS (62; 773–1036), and TianGong-1 (128; 400–2500), HySI (55; 400–1000), HICO (128; 350–1070), DESIS (235; 400–1000), HISUI (185; 400–2500).	Monitoring different crop and soil properties, detecting crop disease, estimating crop properties (chlorophyll, LAI, biomass), assessing crop residues, classifying crop types, investigating soil features	(Apan et al., 2004; Dutta et al., 2006; Moharana and Dutta, 2016; Wu et al., 2010; Bannari et al., 2015; Galloza and Crawford, 2011; Camacho Velasco et al., 2016; Gomez et al., 2008; Zhang et al., 2013)
2.	Airplane-Based Hyperspectral Imaging	AVIRIS (224; 400–2500), CASI (288; 380–1050), HyMap (128; 440–2500), Probe-1 hyperspectral (128; 400–2500), RDACS-H4 hyperspectral (384; 400–2450), AHS-160 hyperspectral Sensor (220; 400–2500), HIS (100; 500–2500), PHI -1 (244; 400–800), APEX (199; 380–2500).	Investigating vegetation Properties, analyzing soil properties and moisture, detecting crop disease and or identifying pest infestation, classifying weeds, mapping crop area	(Estep et al., 2004; Palacios-Orueta and Ustin, 1998; Zhang et al., 2014; Nigam et al., 2019; SW et al., 2019; Ran et al., 2015; Shivers et al., 2018; Haboudane et al., 2002; Liu et al., 2008; Goel et al., 2003)
3.	UAV-Based Hyperspectral Imaging	Headwall Micro- and Nano-Hyperspec (270 (Nano), 324 (Micro); 400–1000), VNIR (224; 400–1000), UHD185-Firefly (125; 450–950), PIKA II sensor (240; 400–900), HySpex VNIR (108; 400–1000).	Estimating LAI and Chlorophyll, Estimating biomass, water, Classification of weeds, Detecting disease	(Lucieer et al., 2014; Gonzalez-Dugo et al., 2015; Hruska et al., 2012; Pablo J. Zarco-Tejada et al., 2013; Glenn et al., 2012; Fenghua et al., 2017; Aasen and Bolten, 2018; Honkavaara et al., 2012; Yue et al., 2017; Pölönen et al., 2013; Kaivosoja et al., 2013; Akhtman et al., 2017; Izzo et al., 2019; Scherrer et al., 2019)
4.	Close-Range (Ground- or Lab-Based) Hyperspectral Imaging	Headwall hyperspectral camera (324; 400–2500), visible and near-infrared HIS camera (360; 440–1000), HySpex hyperspectral camera (360; 960–2500), Integrated a Pika XC hyperspectral line imaging scanner (138; 400–1000), Pika XC-2 hyperspectral camera (447; 400–1000), Cubert UHD185 hyperspectral camera (125; 450–950)	Investigating biochemical components of crops, detecting crop disease, Identifying vegetation species or weeds, Phenotyping analysis and classification of plants, Monitoring soil properties	(Feng et al., 2017; Mohd Asaari et al., 2018; Zhu et al., 2020; Morel et al., 2018; Nagasubramanian et al., 2019; Lopatin et al., 2017; Behmann et al., 2014; Antonucci et al., 2012; Malmir et al., 2019; Eddy et al., 2008)

species of the genus *Acer* L. are widely used in urban landscaping, artificial forests, and ameliorative plantings.

The species: *Acer platanoides* L., *A. saccharinum* L., *A. pseudoplatanus* L. are among the leading species in the landscaping of the inhabited localities of the Rostov region, Russia (Kozlovsky, 2009). Within the genus these species fall into three sections:

A. platanoides refers to the Platanoidea Pax; *A. pseudoplatanus* – to the Acer Pax; and *A. saccharinum* to the Pubra Pax. The species between these sections are distinguished not only phylogenetically and morphologically, but also by the number of pigments in their leaves (Shi-Bao et al., 1992). Shi-Bao et al. (1992) notes that the qualitative composition of anthocyanins in the spring and autumn maple leaves may be an additional trait applicable for their identification at the section level. The species: *Acer platanoides*, *A. saccharinum*, *A. pseudoplatanus* are frost-resistant, drought-resistant, and relatively durable (ontogenesis lasts 50-60 years) under regional conditions. At the same time, the climatic characteristics of the Rostov region are, in general, considered unfavorable for the woody plant growth. Their negative impact may be increased on the background of specific factors of the urban environment. Therefore, urban green spaces are need to be monitored for species composition and plant health. However, large plantations do not allow to perform such monitoring using standard methods (Methodology for the inventory of urban green spaces, 1997).

In the present work, the vegetation indexes have been calculated using a close-range (ground- or lab-based) hyperspectral imaging camera Cubert UHD-185 for the *A. platanoides*, *A. saccharinum* and *A. pseudoplatanus* leaves to test their values for the normal type of distribution, and estimated the difference between the spectral indices of the leaves of different types of maples. The data obtained allowed us to select the most informative indices among them also helped in validation of remote sensing data with real time ground data of vegetation (Goetz, 2009; Hycza et al., 2018; Wang et al., 2021).

2. Materials and methods

2.1. Research region

The research was performed in the Botanic Garden of the Southern Federal University (SFedU), Rostov-on-Don, Russia (Fig. 3). The climate of the Rostov region is temperate continental, arid, average annual rainfall- 548 mm, and most of the precipitation falls in the frost-free period. The summer is hot, the average temperature of July month is +22 ... + 23°C., maximum +40°C. Winter is moderately mild, the average temperature January month is −5°C, the average absolute minimum of air temperature is −20 .- 25°C, the absolute minimum is −32°C. The growing season lasts 216 days (from April 1 to November 4), the frost-free period is 258 days.

2.2. Research methods

Spectral characteristics of plants were studied using Cubert UHD185 hyperspectral camera (Cubert GmbH, Germany) and standard methods (Aasen et al., 2015; Bareth et al., 2015). Plants of *A. platanoides*, *A. saccharinum*, *A. pseudoplatanus* were studied for four years and were grown in the same soil, sunlight, and agronomical conditions of the introductory nursery of the Botanical garden of SFedU. The planting rows were oriented due to north-south directions. At the beginning of the experiment all the plants were at the same stage (virginil) of ontogenesis after that they developed synchronously. The phenologic phases for the maples growing in the Rostov region are presented in Table 2.

Five samples of each maple species were randomly selected from plantings. Each sample was imaged using a hyperspectral camera 5 times. Hyperspectral imaging was performed in 5 repetitions from 12:00 to 14:00 on sunny and cloudless days (August 22, 2019, September 05, 2019, September 13, 2019, September 20, 2019, and September 30, 2019) for what the most sunlit part of the plant crown was chosen. Camera was installed on the south-east side of the trees at a distance of 90 cm and at an angle of 90° to the ground.

Fig. 3. Geographical location of research region in botanical garden of the Southern Federal University (SFedU), Rostov-on-Don, Russia.

Table 2
Phenological phases of development of *A. platanoides, A. saccharinum, A. pseudoplatanus* in the Rostov region.

Phenological phase	Calendar date ±SD (day)		
	A. platanoides	A. pseudoplatanus	A. saccharinum
Blossoming buds	IV.11 ± 1.6	IV.14 ± 1.6	IV.12 ± 2.1
Leaf blossoming	IV.16 ± 1.6	IV.18 ± 1.5	IV.18 ± 2.0
Leaves are fully unfurled	IV.23 ± 1.7	IV.28 ± 1.7	IV.27 ± 2.1
Autumn leaf coloring – beginning	IX.24 ± 2.6	IV.19 ± 4.5	IX.23 ± 3.1
Autumn leaf coloring – mass	X.03 ± 2.5	X.03 ± 6.3	X.08 ± 2.8
Leaf fall – beginning	IX.29 ± 1.8	IX.30 ± 2.9	X.02 ± 2.6
Leaffall – massive	X.13 ± 1.4	X.14 ± 2.7	X.19 ± 2.1
Leaffall – end	X.24 ± 1.6	X.22 ± 3.5	X.31 ± 2.5

Fig. 4. Recording spectral characteristics of *A. platanoides*.

The reflected electromagnetic sun radiation from the leaves was recorded in the range 450–950 nm (Fig. 4). In total, 375 images were obtained. Each image was represented as a single black-and-white image, 1000 × 1000 pixels in size. By 125 hyperspectral images, 50 × 50 pixels in size; the square resolution was up to 35 mm^2. From 60 to 100 spectral profiles measured at the adaxial side of leaves were randomly selected from each image. From 1500 to 2500 profiles were obtained per one experimental variant. Filter Savitsky-Golayfilter (length 12 nm) was applied to decrease the measurement error and to avoid spectral data artifacts at the stage of the preliminary data processing. For each variant of the experiment were calculated 80 vegetation indices. Their titles and formulas for calculations are given in Table 3.

Thus, 1200 sample groups (15 experimental variants x 80 vegetation indices) were performed for the subsequent statistical processing (see Table 4). The sample size of each sample group was from 1500 to 2500 indices values. Sample groups were processed in the statistical calculation environment R (R Core Team), using the «hsdar » package (Lehnert et al., 2019). The following test methods were applied to check the normality of the distribution of vegetation indices values: Norm test Shapiro–Wilk, Pearson's chi-squared, Lilliefors, Cramer–von Mises.Pairwise comparison of vegetation indices values in different *Acer* species were performed using the Wilcox Test for independent samples (Mann Whitney *U* test).

3. Results and discussion

Tests of the normality, i.e., distribution of vegetation indices values for three *Acer* species obtained during the first period of the experiment (August 22, 2019) are shown in Table 3. Results obtained during the study on September 05, 2019, September 13, 2019, September 20, 2019, and September 30, 2019 are shown in supplementary Table 2.

The data processing of the experimental results obtained has shown that only 192 statistical samplings of indices values, from that of a total 1200 (80 indices, 3 Acer species, 5 experiments) were distributed according to the normal law (the case when at least one of

Table 3
Vegetation indices tested for their ability to distinguish different *Acer* species.

	Indexname	Formulafor calculating	References
1	Boochs	D_{703}	(Boochs et al. 1990)
2	Boochs2	D_{720}	(Boochs et al. 1990)
3	CARI	$R_{700} * abs(a * 670 + R_{670} + b)/R_{670} * (a^2 + 1)^{0.5} a = (R_{700} * R_{550})/150, b = R_{550} – (a * 550)$	Kim et al. (1994)
4	Carter2	R_{695}/R_{760}	(Carter, 1994)
5	Carter3	R_{605}/R_{760}	(Carter, 1994)
6	Carter4	R_{710}/R_{760}	(Carter, 1994)
7	Carter5	R_{695}/R_{670}	(Carter, 1994)
8	Carter6	R_{550}	(Carter, 1994)
9	CI	$R_{675} * R_{690}/R^2_{683}$	Zarco-Tejada et al. (2003)
10	CI2	$R_{760}/R_{700} – 1$	Gitelson et al. (2003)
11	ClAInt	$\int_{600nm}^{735nm} R$	Oppelt and Mauser (2004)
12	CRI1	$1/R_{515} – 1/R_{550}$	Gitelson et al. (2003)
13	CRI2	$1/R_{515} – 1/R_{770}$	Gitelson et al. (2003)
14	CRI3	$1/R_{515} – 1/R_{550} * R_{770}$	Gitelson et al. (2003)
15	CRI4	$1/R_{515} – 1/R_{700} * R_{770}$	Gitelson et al. (2003)
16	D1	D_{730}/D_{706}	Zarco-Tejada et al. (2003)
17	D2	D_{705}/D_{722}	Zarco-Tejada et al. (2003)
18	Datt	$(R_{850} – R_{710})/(R_{850} – R_{680})$	Datt (1999)
19	Datt2	R_{850}/R_{710}	Datt (1999)
20	Datt3	D_{754}/D_{704}	Datt (1999)
21	Datt4	$R_{672}/(R_{550} * R_{708})$	Datt (1998)
22	Datt5	R_{672}/R_{550}	Datt (1998)
23	Datt6	$R_{860}/R_{550} * R_{708}$	Datt (1998)
24	DD	$(R_{749} – R_{720}) – (R_{701} – R_{672})$	leMaireetal., (2004)
25	DDn	$2 * (R_{710} – R_{660} – R_{760})$	leMaireetal., (2004)
26	DPI	$D_{688} * D_{710}/D^2_{697}$	Zarco-Tejada et al. (2003)
27	DWSI4	R_{550}/R_{680}	Apan et al. (2004)
28	EGFN	$(max(D_{650:750}) + max(D_{500:550}))/(max(D_{650:750}) + max(D_{500:550}))$	Peñuelas et al. (1994)
29	EGFR	$max(D_{650:750})/max(D_{500:550})$	Peñuelas et al. (1994)
30	EVI	$2,5 * ((R_{800} – R_{670})/(R_{800} – 6 * R_{670} – 7,5 * R_{475} + 1))$	Huete et al. (1997)
31	GI	R_{554}/R_{677}	Smith et al. (1995)
32	Gitelson	$1/R_{700}$	Gitelson et al. (1999)
33	Gitelson2	$(R_{750} – R_{800}/R_{695} – R_{740}) – 1$	Gitelson et al. (2003)
34	GMI1	R_{750}/R_{550}	Gitelson et al. (2003)
35	GMI2	R_{750}/R_{700}	Gitelson et al. (2003)
36	Green NDVI	$(R_{800} – R_{550})/(R_{800} + R_{550})$	Gitelson et al. (1996)
37	Maccioni	$(R_{780} – R_{710})/(R_{780} – R_{680})$	Maccioni et al. (2001)
38	MCARI	$((R_{700} – R_{670}) – 0.2 * (R_{700} – R_{550})) * (R_{700} – R_{670})$	Daughtry et al. (2000)
39	MCARI2	$((R_{700} – R_{670}) – 0.2 * (R_{700} – R_{550})) * (R_{700}/R_{670})$	Daughtry et al. (2000)
40	MPRI	$(R_{515} – R_{530})/(R_{515} + R_{530})$	Hernández-Clemente et al. (2011)
41	MSAVI	$0,5 * (2 * R_{800} + 1–((2 * R_{800} + 1)^2–8 * (R_{800} – R_{670}))^{0,5})$	Qi et al. (1994)
42	mSR2	$(R_{750}/R_{705}) – 1/(R_{750}/R_{705} + 1)^{0,5}$	Chen (1996)
43	MTCI	$(R_{754} – R_{709})/(R_{709} – R_{681})$	Dash and Curran (2004)
44	MTVI	$1,2 * (1,2 * (R_{800} – R_{550})–2,5 * (R_{670} – R_{550}))$	Haboudane et al. (2002)
45	NDVI	$(R_{800} – R_{680})/(R_{800} + R_{680})$	(Tucker, 1979),
46	NDVI2	$(R_{750} – R_{705})/(R_{750} + R_{705})$	Gitelson and Merzlyak (1994)
47	NDVI3	$(R_{682} – R_{553})/(R_{682} + R_{553})$	(S.Gandia et al., 2004)
48	OSAVI	$(1 + 0,16) * (R_{800} – R_{670})/(R_{800} + R_{670} + 0,16)$	Rondeaux et al. (1996)
49	OSAVI2	$(1 + 0,16) * (R_{750} – R_{705})/(R_{750} + R_{705} + 0,16)$	Wu et al. (2008)
50	PARS	R_{746}/R_{513}	Chappelle et al. (1992)
51	PRI	$(R_{531} – R_{570})/(R_{531} + R_{570})$	(Jordan, 1969)
52	PRI_norm	$PRI * (–1)/(RDVI * R_{700}/R_{670})$	(P. J. Zarco-Tejada et al., 2013)
53	PRI*CI2	PRI * CI2	Garrity et al. (2011)
54	PSRI	$(R_{678} – R_{500})/R_{750}$	Merzlyak et al. (1999)
55	PSSR	R_{800}/R_{635}	Blackburn (1998)
56	PSND	$(R_{800} – R_{470})/(R_{800} – R_{470})$	Blackburn (1998)
57	RDVI	$(R_{800} – R_{670})/(R_{800} + R_{670})^{0,5}$	Roujean and Breon (1995)
58	REP_Li	$700 + 40 * ((R_{re} – R_{700})/(R_{740} – R_{700})$ $R_{re} = (R_{670} – R_{780})/2$	Guyot and Baret (1988)
59	SAVI	$(1 + L)/(R_{800} – R_{670})/(R_{800} + R_{670} + L)$	Huete (1988)
60	SPVI	$0,4 * 3,7 * (R_{800} – R_{670}) – 1,2 * ((R_{530} – R_{670})^2)^{0,5}$	(M Vincini et al., 2006)
61	SR	R_{800}/R_{680}	Jordan (1969)
62	SR1	R_{750}/R_{700}	Gitelson and Merzlyak (1997)
63	SR2	R_{752}/R_{690}	Gitelson and Merzlyak (1997)
64	SR3	R_{750}/R_{550}	Gitelson and Merzlyak (1997)
65	SR4	R_{700}/R_{670}	McMurtrey et al. (1994)
66	SR5	R_{675}/R_{700}	Chappelle et al. (1992)
67	SR6	R_{750}/R_{710}	Zarco-Tejada and Miller (1999)

(*continued on next page*)

Table 3 (*continued*)

	Indexname	Formulafor calculating	References
68	SR8	R_{515}/R_{550}	(R et al., 2012)
69	Sum_Dr1	$\sum_{i=626}^{795} D1_i$	Elvidge and Chen (1995)
70	Sum_Dr2	$\sum_{i=680}^{780} D1_i$	Filella and Peñuelas (1994)
71	TCARI	$3 * ((R_{700}- R_{670}) - 0,2 * (R_{700}- R_{550}) *(R_{700}/R_{670}))$	Haboudane et al. (2002)
72	TCARI/OSAVI	TCARI/OSAVI	Haboudane et al. (2002)
73	TCARI2	$3 * ((R_{750}- R_{705}) - 0,2 * (R_{750}- R_{550}) *(R_{750}/R_{705}))$	Wu et al. (2008)
74	TCARI2/OSAVI2	TCARI2/OSAVI2	Wu et al. (2008)
75	TGI	$-0.5 * (190 * (R_{670} - R_{550}) - 120 * (R_{670} - R_{480}))$	Hunt et al. (2013)
76	TVI	$0,5 * (120 * (R_{750}- R_{550})-200 * (R_{670}- R_{550}))$	Broge and Leblanc (2001)
77	Vogelmann	R_{740}/R_{720}	Vogelmann et al. (1993)
78	Vogelmann2	$(R_{734}- R_{747})/(R_{715} + R_{726})$	Vogelmann et al. (1993)
79	Vogelmann3	D_{715}/D_{705}	Vogelmann et al. (1993)
80	Vogelmann4	$(R_{734}- R_{747})/(R_{715} + R_{720})$	Vogelmann et al. (1993)

Notes: R_{xxx}: Reflectance at the wavelength “xxx”, D_{xxx}: First derivation of reflectance values at the wavelength “xxx”.

the four test methods confirmed the normal distribution). None of the test methods confirmed the normal type of distribution for any of the vegetation indices simultaneously for all three species of *Acer* in all five experiments. It makes impossible to use the parametric criteria to compare the values of vegetation indices of different *Acer* species. We applied a non-parametric Wilcox Test for independent samples (Mann Whitney *U* test). Mean values of the vegetation indices (X±SD) and results of the pairwise comparison or the vegetation indices (by the Wilcox Test) are presented in Table 5.

Number of the vegetation indices, the values of which were significantly differed in the compared *Acer* species pairs according to the Wilcox Test, appeared to be large (Table 6).

At the same time, we found 40 vegetation indices that significantly differed between species in their values simultaneously in all pairs: *A. saccharinum* vs. *A. platanoides*, *A. saccharinum* vs. *A. pseudoplatanus* and *A. platanoides* vs. *A. pseudoplatanus* in all five observation periods. They are: Carter2, Carter4, Carter5, CI, CI2, CRI2, CRI3, CRI4, D1, Datt2, Datt4, Datt5, Datt6, DWSI4, EGFN, EGFR, GI, Gitelson2, GMI1, GMI2, Green NDVI, MCARI, MCARI2, mSR2, MTVI, NDVI2, OSAVI2, PRI, PRI*CI2, PRI_norm, RDVI, REP_Li, SR1, SR3, Sum_Dr1, TGI, TVI, Vogelmann2, Vogelmann3 and Vogelmann4. When analyzing the nature of the observed differences, it was found that for some indices their values in the compared pairs of maples retained the same trend in all five experiments (Fig. 5a). For other indices, the trends of their values in some periods of observation changed to the opposite (Fig. 5b). We excluded the second group of vegetation indices as unreliable since there is a possibility that the observed difference in the indices values in the compared pairs may be a result of the influence of random factors. Vegetation indices suitable to identify (in our opinion) the *Acer* species are listed in Table 7.

Most of the vegetation indices, which enable to distinguish between different maple species, were found to be designated to the calculations on basis of the 475-860 nm spectral band. Indices calculated using the channels N 55, 62, 74, 75 were found to be more informative. They are: Boochs2, Carter5, CI2, CRI4, Datt3, Datt5, EVI, GMI1, GMI2, MCARI2, mSR2, MTCI, NDVI2, OSAVI2, PARS, REP_Li, SR1, SR2, SR3, SR4, SR5, TCARI2, TGI, Vogelmann2, Vogelmann4 (Table 8).

4. Conclusion

In our study, values of 80 vegetation indices for the leaves of three maple species, *A. platanoides*, *A. pseudoplatanus* and *A. saccharinum* have been calculated. It was observed, that most of the studied indices values were not distributed according to the normal law. For this reason, we used the nonparametric Wilcox Test criterion for independent samples. Mann Whitney *U* test for parawise comparisons of different indices for *Acer* species. Forty vegetation indices were found to be significantly differed simultaneously in the following pairs: *A. saccharinum* vs. *A. platanoides, A. saccharinum*vs vs. *A. pseudoplatanus* and *A. platanoides* vs. *A. pseudoplatanus* in all experiments.They are: Carter2, Carter4, Carter5, CI, CI2, CRI2, CRI3, CRI4, D1, Datt2, Datt4, Datt5, Datt6, DWSI4, EGFN, EGFR, GI, Gitelson2, GMI1, GMI2, Green NDVI, MCARI, MCARI2, mSR2, MTVI, NDVI2, OSAVI2, PRI, PRI*CI2, PRI_norm, RDVI, REP_Li, SR1, SR3, Sum_Dr1, TGI, TVI, Vogelmann2, Vogelmann3 and Vogelmann4. From the data obtained, we have selected the following indices reliable for the *Acer* species distinguishing: For the pair *A. platanoides* vs. *A. pseudoplatanus* – Boochs2, MCARI2, TCARI2, Vogelmann2 and Vogelmann4; for the pair *A. platanoides* vs. *A. saccharinum* – Carter2, Carter3, Carter4, Carter5, CI, CI2, CRI3, CRI4, Datt, Datt2, Datt3, Datt5, DDn, DWSI4, EGFN, EGFR, EVI, GI, GMI1, GMI2, Green NDVI, Maccioni, MCARI2, mSR2, MTCI, NDVI2, NDVI3, OSAVI2, PARS, PSSR, REP_Li, SR1, SR2, SR3, SR4, SR8, Vogelmann2 and Vogelmann4; for the pair

Table 4
Shapiro–Wilk (1), Pearson's chi-squared (2), Lilliefors (3), Cramér–von Mises (4) norm tests of the VIs values for *A. platanoides*, *A. pseudoplatanus* and *A. saccharinum*.

Test	1	2	3	4	1	2	3	4	1	2	3	4
VI	*A. platanoides*				*A. pseudoplatanus*				*A. saccharinum*			
Boochs	0.00	0.00	0.00	0.00	0.10	0.14	0.77	0.64	0.45	0.44	0.62	0.69
Boochs2	0.04	0.02	0.05	0.02	0.00	0.13	0.20	0.05	0.01	0.03	0.02	0.00
CARI	0.00	0.05	0.01	0.00	0.00	0.00	0.00	0.00	0.00	0.00	0.00	0.00
Carter2	0.00	0.00	0.00	0.00	0.00	0.00	0.00	0.00	0.00	0.00	0.00	0.00
Carter3	0.00	0.00	0.00	0.00	0.00	0.00	0.00	0.00	0.00	0.00	0.00	0.00
Carter4	0.00	0.00	0.00	0.00	0.00	0.01	0.04	0.02	0.00	0.00	0.00	0.00
Carter5	0.00	0.02	0.03	0.01	0.00	0.00	0.00	0.00	0.00	0.00	0.00	0.00
Carter6	0.00	0.00	0.00	0.00	0.00	0.00	0.02	0.01	0.00	0.00	0.00	0.00
CI	0.00	0.05	0.00	0.00	0.20	0.26	0.47	0.49	0.04	0.07	0.01	0.01
CI2	0.00	0.00	0.00	0.00	0.00	0.39	0.01	0.01	0.03	0.32	0.76	0.58
ClAInt	0.00	0.00	0.00	0.00	0.00	0.00	0.01	0.00	0.00	0.04	0.01	0.00
CRI1	0.00	0.00	0.00	0.00	0.00	0.00	0.00	0.00	0.00	0.01	0.00	0.00
CRI2	0.00	0.00	0.00	0.00	0.00	0.00	0.00	0.00	0.01	0.05	0.02	0.01
CRI3	0.00	0.00	0.00	0.00	0.10	0.53	0.28	0.20	0.01	0.01	0.01	0.01
CRI4	0.00	0.00	0.00	0.00	0.00	0.48	0.02	0.02	0.03	0.49	0.76	0.80
D1	0.00	0.00	0.00	0.00	0.00	0.00	0.00	0.00	0.49	0.98	0.62	0.68
D2	0.00	0.00	0.00	0.00	0.00	0.00	0.00	0.00	0.00	0.00	0.00	0.00
Datt	0.00	0.00	0.00	0.00	0.00	0.00	0.00	0.00	0.00	0.00	0.00	0.00
Datt2	0.00	0.00	0.00	0.00	0.00	0.01	0.00	0.00	0.04	0.46	0.08	0.19
Datt3	0.00	0.08	0.04	0.01	0.00	0.47	0.06	0.01	0.55	0.22	0.57	0.68
Datt4	0.00	0.00	0.00	0.00	0.00	0.00	0.00	0.00	0.00	0.28	0.42	0.41
Datt5	0.00	0.06	0.02	0.01	0.01	0.00	0.17	0.07	0.15	0.59	0.42	0.37
Datt6	0.00	0.00	0.00	0.00	0.00	0.00	0.00	0.00	0.00	0.10	0.01	0.00
DD	0.00	0.00	0.00	0.00	0.00	0.12	0.04	0.01	0.00	0.00	0.00	0.00
DDn	0.00	0.05	0.00	0.00	0.00	0.01	0.02	0.01	0.00	0.00	0.00	0.00
DPI	0.03	0.11	0.17	0.06	0.00	0.01	0.00	0.00	0.73	0.73	0.68	0.88
DWSI4	0.00	0.00	0.00	0.00	0.00	0.00	0.00	0.00	0.11	0.47	0.28	0.32
EGFN	0.02	0.34	0.13	0.03	0.00	0.00	0.00	0.00	0.00	0.03	0.18	0.05
EGFR	0.00	0.12	0.01	0.00	0.00	0.00	0.00	0.00	0.00	0.01	0.00	0.00
EVI	0.00	0.00	0.00	0.00	0.00	0.00	0.00	0.00	0.00	0.00	0.00	0.00
GI	0.00	0.00	0.00	0.00	0.00	0.00	0.00	0.00	0.09	0.44	0.30	0.28
Gitelson	0.00	0.00	0.00	0.00	0.00	0.00	0.05	0.01	0.00	0.39	0.01	0.00
Gitelson2	0.00	0.03	0.00	0.00	0.12	0.61	0.10	0.39	0.44	0.88	0.30	0.57
GMI1	0.00	0.00	0.00	0.00	0.21	0.89	0.45	0.30	0.01	0.03	0.01	0.01
GMI2	0.00	0.00	0.00	0.00	0.00	0.36	0.01	0.01	0.03	0.08	0.83	0.54
Green NDVI	0.00	0.01	0.00	0.00	0.00	0.08	0.04	0.00	0.00	0.00	0.00	0.00
Maccioni	0.00	0.00	0.00	0.00	0.00	0.00	0.00	0.00	0.00	0.00	0.00	0.00
MCARI	0.00	0.01	0.03	0.00	0.00	0.00	0.00	0.00	0.00	0.00	0.00	0.00
MCARI2	0.00	0.00	0.00	0.00	0.00	0.00	0.00	0.00	0.01	0.19	0.20	0.11
MPRI	0.00	0.00	0.00	0.00	0.00	0.15	0.01	0.00	0.00	0.00	0.00	0.00
MSAVI	0.00	0.00	0.00	0.00	0.00	0.00	0.00	0.00	0.00	0.01	0.00	0.00
mSR2	0.00	0.00	0.00	0.00	0.02	0.09	0.06	0.04	0.04	0.18	0.31	0.29
MTCI	0.00	0.00	0.00	0.00	0.00	0.23	0.17	0.03	0.03	0.70	0.48	0.28
MTVI	0.00	0.00	0.00	0.00	0.00	0.00	0.00	0.00	0.01	0.22	0.11	0.08
NDVI	0.00	0.00	0.00	0.00	0.00	0.01	0.00	0.00	0.00	0.01	0.00	0.00
NDVI2	0.00	0.00	0.00	0.00	0.03	0.19	0.43	0.55	0.00	0.00	0.00	0.00
NDVI3	0.00	0.00	0.00	0.00	0.04	0.14	0.28	0.19	0.21	0.52	0.62	0.52
OSAVI	0.00	0.00	0.00	0.00	0.00	0.00	0.00	0.00	0.00	0.03	0.00	0.00
OSAVI2	0.00	0.00	0.00	0.00	0.03	0.27	0.43	0.54	0.00	0.00	0.00	0.00
PARS	0.00	0.00	0.00	0.00	0.09	0.36	0.58	0.62	0.13	0.38	0.51	0.30
PRI	0.00	0.00	0.00	0.00	0.06	0.05	0.22	0.32	0.00	0.00	0.00	0.00
PRI_norm	0.00	0.02	0.01	0.00	0.09	0.08	0.00	0.04	0.00	0.06	0.02	0.00
PRI*CI2	0.00	0.00	0.00	0.00	0.00	0.00	0.00	0.00	0.00	0.00	0.16	0.02
PSRI	0.00	0.00	0.00	0.00	0.00	0.01	0.00	0.00	0.00	0.07	0.05	0.01
PSSR	0.00	0.00	0.00	0.00	0.01	0.25	0.13	0.09	0.00	0.01	0.02	0.00
PSND	0.00	0.00	0.00	0.00	0.00	0.00	0.00	0.00	0.00	0.03	0.01	0.01
RDVI	0.00	0.00	0.00	0.00	0.00	0.00	0.00	0.00	0.01	0.03	0.05	0.04
REP_Li	0.00	0.00	0.00	0.00	0.00	0.00	0.00	0.00	0.00	0.00	0.00	0.00
SAVI	0.00	0.00	0.00	0.00	0.00	0.00	0.00	0.00	0.00	0.01	0.00	0.00
SPVI	0.00	0.00	0.00	0.00	0.00	0.00	0.00	0.00	0.14	0.05	0.56	0.50
SR	0.00	0.00	0.00	0.00	0.02	0.07	0.07	0.23	0.08	0.68	0.93	0.76
Test	1	2	3	4	1	2	3	4	1	2	3	4
VI	*A. platanoides*				*A. pseudoplatanus*				*A. saccharinum*			
SR1	0.00	0.00	0.00	0.00	0.00	0.36	0.01	0.01	0.03	0.08	0.83	0.54
SR2	0.00	0.00	0.00	0.00	0.04	0.21	0.62	0.49	0.02	0.03	0.78	0.58
SR3	0.00	0.00	0.00	0.00	0.21	0.89	0.45	0.30	0.01	0.03	0.01	0.01
SR4	0.00	0.00	0.00	0.00	0.00	0.00	0.00	0.00	0.00	0.01	0.00	0.00
SR5	0.00	0.00	0.00	0.00	0.00	0.01	0.00	0.00	0.01	0.03	0.36	0.53
SR6	0.00	0.00	0.00	0.00	0.00	0.03	0.02	0.01	0.04	0.17	0.57	0.49
SR8	0.03	0.26	0.05	0.10	0.00	0.00	0.00	0.00	0.25	0.59	0.75	0.48
Sum_Dr1	0.00	0.00	0.00	0.00	0.00	0.00	0.00	0.00	0.00	0.04	0.10	0.01
Sum_Dr2	0.00	0.00	0.00	0.00	0.00	0.00	0.00	0.00	0.06	0.40	0.06	0.13
TCARI	0.00	0.00	0.00	0.00	0.00	0.00	0.00	0.00	0.00	0.00	0.01	0.00
TCARI/OSAVI	0.00	0.00	0.00	0.00	0.00	0.02	0.22	0.05	0.00	0.00	0.00	0.00
TCARI2	0.00	0.00	0.00	0.00	0.00	0.00	0.00	0.01	0.01	0.13	0.01	0.00
TCARI2/OSAVI2	0.00	0.00	0.00	0.00	0.00	0.01	0.10	0.04	0.00	0.12	0.05	0.01
TGI	0.00	0.00	0.00	0.00	0.00	0.00	0.00	0.00	0.00	0.00	0.00	0.00
TVI	0.00	0.00	0.00	0.00	0.00	0.00	0.00	0.00	0.00	0.01	0.05	0.01
Vogelmann	0.00	0.00	0.00	0.00	0.00	0.00	0.00	0.00	0.02	0.20	0.27	0.14
Vogelmann2	0.00	0.00	0.00	0.00	0.00	0.01	0.00	0.00	0.00	0.01	0.19	0.19
Vogelmann3	0.00	0.00	0.00	0.00	0.38	0.27	0.93	0.96	0.02	0.14	0.15	0.05
Vogelmann4	0.00	0.00	0.00	0.00	0.00	0.01	0.00	0.00	0.00	0.00	0.31	0.11

Notes: Green color indicates the values for which $p > 0.05$

A. pseudoplatanus vs. *A. saccharinum* – Carter3, Carter5, CRI3, Datt5, Datt6, DWSI4, EGFN, EGFR, GI, GMI1, Green NDVI, NDVI3, PARS, SR3, SR4, SR5, SR8 and TGI. Thus, the species *A. platanoides*, *A. pseudoplatanus*, and *A. saccharinum* can be identified using vegetation indices calculated from hyperspectral imaging data in this study. Also, the results of the study may be used to develop approaches for

Table 5
Statistical characteristics of vegetation indices (VIs) values of *A. platanoides* (pl), *A. pseudoplatanus* (ps) and *A. saccharinum* (sa).

Number of experiment		1	2	3	4	5
VI	Species	Mean of VI value ± SD				
Boochs	Pl	6.978±0.037	5.898±0.044	3.472±0.024	7.164±0.025	15.023±0.076
	Ps	6.483±0.053	5.618±0.034	3.627±0.029	6.547±0.034	8.720±0.166
	Sa	6.984±0.066	6.987±0.064	3.208±0.035	6.795±0.023	2.901±0.019
Boochs2	Pl	7.350±0.031	6.480±0.029	3.477±0.025	5.386±0.020	4.652±0.095
	Ps	6.501±0.057	5.172±0.028	3.463±0.026	4.884±0.036	4.149±0.040
	Sa	5.970±0.060	6.680±0.061	2.696±0.023	4.526±0.041	2.126±0.019
CARI	Pl	133.021±0.976	111.830±1.029	64.813±0.541	199.140±1.282	483.395±3.797
	Ps	134.178±1.818	135.792±1.233	73.153±0.751	201.679±1.956	257.529±6.266
	Sa	204.904±3.124	185.935±2.273	99.561±1.561	281.523±2.207	146.200±1.621
Carter2	Pl	0.237±0.001	0.234±0.001	0.272±0.001	0.320±0.001	0.394±0.002
	Ps	0.260±0.002	0.287±0.002	0.285±0.002	0.392±0.003	0.376±0.003
	Sa	0.300±0.003	0.270±0.003	0.336±0.003	0.438±0.004	0.445±0.004
Carter3	Pl	0.126±0.001	0.130±0.001	0.162±0.001	0.130±0.001	0.176±0.001
	Ps	0.144±0.001	0.137±0.001	0.157±0.001	0.179±0.002	0.142±0.001
	Sa	0.153±0.002	0.142±0.002	0.182±0.002	0.208±0.003	0.217±0.003
Carter4	Pl	0.485±0.002	0.472±0.002	0.512±0.002	0.590±0.001	0.668±0.001
	Ps	0.513±0.003	0.541±0.002	0.532±0.002	0.637±0.002	0.623±0.002
	Sa	0.568±0.004	0.528±0.003	0.589±0.004	0.680±0.003	0.695±0.003
Carter5	Pl	2.601±0.010	2.438±0.010	2.138±0.016	3.470±0.019	3.189±0.014
	Ps	2.579±0.024	3.254±0.037	2.330±0.015	3.006±0.027	3.554±0.031
	Sa	3.499±0.026	3.302±0.022	3.370±0.030	3.733±0.024	3.738±0.024
Carter6	Pl	17.827±0.122	16.439±0.156	11.210±0.129	18.797±0.129	50.354±0.362
	Ps	18.667±0.163	16.720±0.189	11.269±0.112	23.659±0.257	26.206±0.662
	Sa	24.595±0.318	23.288±0.337	12.852±0.218	31.632±0.445	17.529±0.246
CI	Pl	1.139±0.001	1.134±0.001	1.107±0.001	1.005±0.001	1.057±0.001
	Ps	1.134±0.002	1.086±0.002	1.122±0.001	0.994±0.002	0.987±0.002
	Sa	1.096±0.003	1.109±0.002	1.062±0.003	0.925±0.002	0.963±0.002
CI2	Pl	2.297±0.015	2.363±0.018	1.922±0.014	1.477±0.009	1.066±0.008
	Ps	2.016±0.021	1.788±0.015	1.834±0.018	1.175±0.013	1.259±0.016
	Sa	1.612±0.024	1.954±0.027	1.464±0.022	1.005±0.014	0.898±0.014
ClAInt	Pl	905.470±5.753	822.368±7.012	541.270±5.362	952.301±4.356	2275.598±12.130
	Ps	914.563±6.253	793.924±7.544	536.768±4.137	1133.474±8.391	1476.545±34.419
	Sa	959.942±11.061	990.147±12.156	500.560±6.924	1297.647±13.942	681.455±10.478
CRI1	Pl	0.029±0.000	0.036±0.000	0.048±0.001	0.026±0.000	0.013±0.000
	Ps	0.024±0.000	0.039±0.001	0.044±0.001	0.022±0.000	0.032±0.001
	Sa	0.030±0.000	0.033±0.001	0.060±0.001	0.022±0.000	0.037±0.001

Number of experiment		1	2	3	4	5
VI	Species	Mean of VI value ± SD				
CRI2	Pl	0.055±0.000	0.064±0.001	0.089±0.002	0.053±0.000	0.023±0.000
	Ps	0.048±0.000	0.069±0.001	0.082±0.001	0.046±0.001	0.066±0.001
	Sa	0.044±0.001	0.050±0.001	0.093±0.002	0.039±0.001	0.059±0.001
CRI3	Pl	-5.934±0.025	-5.783±0.031	-4.943±0.028	-5.171±0.025	-4.178±0.016
	Ps	-5.336±0.035	-5.131±0.034	-4.811±0.031	-4.509±0.038	-5.730±0.034
	Sa	-3.992±0.041	-4.742±0.054	-3.841±0.044	-3.773±0.037	-3.029±0.032
CRI4	Pl	-3.264±0.015	-3.300±0.018	-2.811±0.013	-2.428±0.009	-2.070±0.008
	Ps	-2.991±0.021	-2.715±0.014	-2.733±0.017	-2.151±0.013	-2.235±0.014
	Sa	-2.564±0.024	-2.901±0.026	-2.337±0.020	-1.979±0.014	-1.806±0.013
D1	Pl	0.647±0.004	0.656±0.005	0.668±0.005	0.461±0.002	0.123±0.003
	Ps	0.627±0.006	0.601±0.003	0.603±0.005	0.556±0.003	0.454±0.004
	Sa	0.533±0.006	0.574±0.006	0.546±0.006	0.575±0.002	0.378±0.004
D2	Pl	1.063±0.005	0.998±0.005	1.106±0.007	1.517±0.006	4.305±0.172
	Ps	1.102±0.008	1.205±0.007	1.156±0.008	1.438±0.007	1.614±0.018
	Sa	1.248±0.011	1.155±0.010	1.270±0.011	1.575±0.012	1.427±0.010
Datt	Pl	0.596±0.001	0.620±0.002	0.599±0.002	0.510±0.001	0.463±0.001
	Ps	0.581±0.003	0.550±0.002	0.575±0.002	0.511±0.002	0.537±0.002
	Sa	0.495±0.004	0.553±0.003	0.486±0.003	0.462±0.002	0.366±0.003
Datt2	Pl	2.174±0.008	2.264±0.010	2.073±0.008	1.802±0.005	1.648±0.004
	Ps	2.086±0.011	1.951±0.008	2.010±0.009	1.752±0.007	1.866±0.007
	Sa	1.793±0.012	2.033±0.014	1.763±0.012	1.640±0.007	1.422±0.007
Datt3	Pl	0.186±0.002	0.228±0.002	0.168±0.002	0.079±0.001	0.339±0.005
	Ps	0.181±0.003	0.110±0.002	0.174±0.003	0.043±0.002	0.211±0.006
	Sa	0.113±0.003	0.159±0.003	0.110±0.003	-0.033±0.002	0.104±0.003
Datt4	Pl	0.012±0.000	0.015±0.000	0.026±0.000	0.010±0.000	0.004±0.000
	Ps	0.013±0.000	0.012±0.000	0.023±0.000	0.011±0.000	0.010±0.000
	Sa	0.007±0.000	0.008±0.000	0.016±0.000	0.007±0.000	0.011±0.000
Datt5	Pl	0.543±0.002	0.565±0.002	0.667±0.003	0.523±0.002	0.523±0.002
	Ps	0.558±0.004	0.502±0.005	0.587±0.004	0.617±0.005	0.611±0.005
	Sa	0.351±0.002	0.387±0.002	0.401±0.004	0.454±0.002	0.403±0.003
Datt6	Pl	0.137±0.001	0.169±0.002	0.213±0.003	0.102±0.001	0.036±0.000
	Ps	0.122±0.001	0.141±0.002	0.196±0.002	0.089±0.001	0.111±0.002
	Sa	0.081±0.002	0.105±0.002	0.168±0.004	0.066±0.001	0.086±0.001
DD	Pl	5.282±0.211	6.122±0.200	2.753±0.159	-9.954±0.215	-45.479±0.487
	Ps	2.232±0.394	-1.742±0.237	0.294±0.175	-13.333±0.369	-22.500±0.758
	Sa	-8.265±0.559	-2.414±0.434	-5.387±0.253	-23.139±0.503	-14.289±0.271
DDn	Pl	-125.509±0.501	-113.509±0.538	-66.829±0.508	-97.446±0.287	-186.421±0.754
	Ps	-113.816±0.962	-91.698±0.649	-63.630±0.437	-98.081±0.555	-131.059±2.718
	Sa	-101.571±0.816	-113.196±0.837	-48.047±0.350	-92.283±0.337	-39.508±0.255
DPI	Pl	0.845±0.003	0.897±0.003	0.799±0.004	0.941±0.002	0.722±0.005
	Ps	0.829±0.004	0.888±0.003	0.798±0.003	0.860±0.003	0.883±0.006
	Sa	0.798±0.006	0.853±0.004	0.803±0.005	0.837±0.004	0.882±0.005
DWSI4	Pl	1.587±0.005	1.539±0.005	1.345±0.005	1.384±0.004	1.457±0.005
	Ps	1.574±0.010	1.629±0.010	1.480±0.007	1.242±0.006	1.148±0.009
	Sa	2.188±0.013	2.051±0.010	1.952±0.013	1.461±0.006	1.715±0.009
EGFN	Pl	0.740±0.001	0.717±0.001	0.704±0.002	0.682±0.002	0.638±0.001
	Ps	0.715±0.003	0.672±0.002	0.680±0.002	0.634±0.002	0.708±0.002
	Sa	0.534±0.004	0.577±0.004	0.526±0.003	0.514±0.003	0.436±0.003
EGFR	Pl	6.767±0.034	6.168±0.033	5.874±0.037	5.439±0.033	4.599±0.022
	Ps	6.473±0.075	5.328±0.047	5.379±0.047	4.580±0.036	5.912±0.038
	Sa	3.369±0.033	4.000±0.048	3.300±0.033	3.155±0.022	2.519±0.016
EVI	Pl	-8.714±0.183	-2.932±0.342	-3.127±0.057	-6.193±0.227	-6.147±0.101
	Ps	-6.101±0.137	-0.688±0.332	-4.802±0.100	-3.069±0.076	-0.410±0.577
	Sa	-8.057±0.420	2.704±0.606	-3.064±0.499	-4.434±0.258	-4.343±0.116
GI	Pl	1.728±0.006	1.662±0.005	1.436±0.007	1.598±0.005	1.667±0.006
	Ps	1.712±0.012	1.846±0.014	1.589±0.009	1.419±0.008	1.343±0.010
	Sa	2.508±0.016	2.322±0.012	2.252±0.017	1.734±0.007	2.043±0.012
Gitelson	Pl	0.032±0.000	0.039±0.000	0.055±0.001	0.025±0.000	0.010±0.000
	Ps	0.031±0.000	0.035±0.000	0.052±0.000	0.022±0.000	0.023±0.000
	Sa	0.027±0.000	0.029±0.000	0.054±0.001	0.019±0.000	0.035±0.001
Gitelson2	Pl	0.046±0.034	-0.273±0.036	-1.987±0.031	-0.329±0.017	12.754±0.192
	Ps	-0.458±0.047	-1.001±0.034	-2.203±0.023	-0.648±0.029	6.769±0.445
	Sa	-0.708±0.043	-0.058±0.048	-2.327±0.027	-0.837±0.026	-2.436±0.018
GMI1	Pl	5.743±0.023	5.614±0.029	4.895±0.028	5.115±0.024	3.914±0.017
	Ps	5.161±0.032	5.092±0.033	4.775±0.030	4.430±0.036	5.466±0.036

Number of experiment		1	2	3	4	5
VI	Species	Mean of VI value ± SD				
	Sa	3.948±0.040	4.652±0.051	3.858±0.044	3.775±0.037	3.093±0.032
GMI2	Pl	3.198±0.014	3.245±0.017	2.847±0.013	2.443±0.009	1.956±0.008
	Ps	2.929±0.019	2.737±0.014	2.755±0.016	2.155±0.013	2.187±0.016
	Sa	2.562±0.023	2.876±0.025	2.416±0.021	2.009±0.014	1.863±0.013
Green NDVI	Pl	0.716±0.001	0.718±0.001	0.676±0.002	0.691±0.001	0.635±0.001
	Ps	0.691±0.002	0.681±0.002	0.669±0.002	0.641±0.002	0.720±0.001
	Sa	0.604±0.003	0.651±0.003	0.590±0.004	0.579±0.003	0.505±0.004
Maccioni	Pl	0.590±0.001	0.606±0.002	0.585±0.002	0.493±0.001	0.432±0.001
	Ps	0.569±0.003	0.539±0.002	0.560±0.002	0.477±0.002	0.495±0.002
	Sa	0.498±0.003	0.540±0.003	0.487±0.003	0.426±0.003	0.378±0.003
MCARI	Pl	67.330±0.550	53.600±0.520	26.640±0.289	115.854±0.938	255.445±2.256
	Ps	68.555±1.326	73.426±0.980	34.057±0.482	105.227±1.450	130.595±2.691
	Sa	125.196±2.057	109.312±1.400	58.889±1.081	164.613±1.203	86.023±0.843
MCARI2	Pl	107.327±0.668	99.961±0.688	48.317±0.456	64.757±0.422	74.234±0.700
	Ps	88.511±1.183	68.648±0.559	44.066±0.452	52.790±0.665	56.971±0.646
	Sa	72.229±1.153	92.253±1.212	30.270±0.374	47.068±0.659	15.879±0.250
MPRI	Pl	11.369±0.089	10.157±0.106	7.375±0.108	12.214±0.098	30.226±0.221
	Ps	12.280±0.103	10.268±0.142	6.917±0.072	15.929±0.192	15.490±0.392
	Sa	13.822±0.191	13.364±0.212	6.865±0.129	19.363±0.280	10.153±0.157
MSAVI	Pl	0.910±0.001	0.906±0.001	0.869±0.001	0.910±0.001	0.886±0.001
	Ps	0.900±0.001	0.906±0.001	0.885±0.001	0.869±0.002	0.901±0.001
	Sa	0.915±0.001	0.922±0.001	0.903±0.001	0.883±0.002	0.880±0.001
mSR2	Pl	1.974±0.010	2.033±0.012	1.756±0.010	1.419±0.007	1.022±0.006
	Ps	1.786±0.015	1.653±0.010	1.670±0.012	1.222±0.010	1.231±0.012
	Sa	1.499±0.017	1.738±0.018	1.412±0.016	1.103±0.011	0.988±0.010
MTCI	Pl	1.495±0.009	1.601±0.010	1.476±0.012	0.997±0.006	0.681±0.004
	Ps	1.386±0.015	1.231±0.009	1.323±0.012	0.919±0.008	0.897±0.009
	Sa	1.041±0.014	1.253±0.015	1.022±0.013	0.764±0.008	0.655±0.008
MTVI	Pl	153.574±0.585	134.826±0.701	75.818±0.412	150.753±0.405	323.416±1.721
	Ps	142.803±1.003	123.938±0.641	78.778±0.506	146.763±0.693	214.568±4.808
	Sa	157.950±1.280	165.591±1.309	73.928±0.704	170.850±0.689	74.795±0.544
NDVI	Pl	0.809±0.001	0.805±0.001	0.746±0.002	0.771±0.001	0.733±0.001
	Ps	0.790±0.002	0.785±0.002	0.765±0.002	0.695±0.002	0.744±0.002
	Sa	0.797±0.002	0.817±0.002	0.766±0.003	0.686±0.003	0.684±0.003
NDVI2	Pl	0.426±0.002	0.435±0.002	0.395±0.002	0.334±0.001	0.239±0.002
	Ps	0.398±0.002	0.374±0.002	0.376±0.002	0.286±0.002	0.285±0.003
	Sa	0.345±0.003	0.383±0.003	0.325±0.003	0.255±0.003	0.231±0.003
NDVI3	Pl	-0.195±0.002	-0.184±0.001	-0.122±0.002	-0.106±0.001	-0.138±0.002
	Ps	-0.190±0.003	-0.187±0.003	-0.168±0.002	-0.056±0.002	-0.005±0.004
	Sa	-0.326±0.003	-0.301±0.002	-0.271±0.003	-0.126±0.002	-0.201±0.002
OSAVI	Pl	0.969±0.001	0.962±0.002	0.893±0.002	0.967±0.001	0.923±0.001
	Ps	0.949±0.002	0.960±0.002	0.920±0.002	0.893±0.003	0.951±0.002
	Sa	0.978±0.002	0.991±0.002	0.955±0.003	0.918±0.003	0.911±0.003
OSAVI2	Pl	0.493±0.002	0.503±0.002	0.457±0.002	0.387±0.002	0.278±0.002
	Ps	0.461±0.003	0.433±0.002	0.435±0.002	0.331±0.003	0.331±0.003
	Sa	0.399±0.004	0.443±0.004	0.376±0.004	0.295±0.003	0.268±0.003
PARS	Pl	8.827±0.044	8.814±0.054	7.388±0.069	7.920±0.049	6.478±0.031
	Ps	7.722±0.049	8.418±0.075	7.206±0.047	6.709±0.067	9.140±0.076
	Sa	7.186±0.073	8.338±0.092	6.832±0.085	6.362±0.064	5.493±0.058
PRI	Pl	0.004±0.001	-0.003±0.001	-0.012±0.001	0.040±0.001	-0.003±0.001
	Ps	-0.002±0.001	0.026±0.001	-0.004±0.001	0.009±0.001	-0.019±0.002
	Sa	0.022±0.001	0.018±0.001	0.008±0.001	0.015±0.001	0.025±0.001
PRI_norm	Pl	0.014±0.002	0.003±0.002	-0.018±0.002	0.061±0.001	-0.002±0.001
	Ps	-0.001±0.002	0.045±0.002	-0.006±0.001	0.010±0.001	-0.009±0.002
	Sa	0.042±0.002	0.036±0.002	0.019±0.002	0.026±0.001	0.026±0.001
PRI*CI2	Pl	0.000±0.000	0.000±0.000	0.001±0.000	-0.001±0.000	0.000±0.000
	Ps	0.000±0.000	-0.001±0.000	0.000±0.000	0.000±0.000	0.001±0.000
	Sa	-0.001±0.000	0.000±0.000	0.000±0.000	0.000±0.000	-0.001±0.000
PSRI	Pl	0.829±0.001	0.845±0.001	0.807±0.002	0.823±0.001	0.823±0.001
	Ps	0.807±0.001	0.821±0.002	0.808±0.001	0.786±0.002	0.863±0.001
	Sa	0.825±0.001	0.864±0.001	0.841±0.002	0.823±0.002	0.798±0.002
PSSR	Pl	0.007±0.000	0.016±0.000	0.026±0.000	0.023±0.000	0.040±0.000
	Ps	0.004±0.000	0.015±0.000	0.015±0.000	0.044±0.001	0.063±0.001
	Sa	0.004±0.001	0.012±0.000	0.017±0.001	0.056±0.001	0.038±0.001
PSND	Pl	9.754±0.061	9.370±0.069	7.341±0.066	9.768±0.068	7.231±0.037

Number of experiment		1	2	3	4	5
VI	Species	Mean of VI value ± SD				
	Ps	8.297±0.068	9.649±0.100	7.540±0.060	7.363±0.085	9.505±0.106
	Sa	8.242±0.104	9.257±0.125	7.274±0.108	7.382±0.100	5.862±0.078
RDVI	Pl	9.037±0.016	8.478±0.022	6.111±0.013	8.845±0.011	12.489±0.033
	Ps	8.572±0.032	7.940±0.017	6.319±0.018	8.475±0.017	10.182±0.107
	Sa	8.751±0.032	9.100±0.036	5.861±0.028	8.884±0.014	5.506±0.012
REP_Li	Pl	716.384±0.057	717.083±0.062	716.282±0.068	711.746±0.074	710.480±0.122
	Ps	715.648±0.116	713.700±0.094	715.131±0.100	709.509±0.161	711.670±0.153
	Sa	711.797±0.175	713.911±0.134	710.351±0.187	704.230±0.268	702.412±0.274
SAVI	Pl	1.250±0.001	1.239±0.002	1.149±0.003	1.247±0.002	1.192±0.001
	Ps	1.224±0.002	1.237±0.003	1.183±0.002	1.152±0.004	1.227±0.003
	Sa	1.260±0.002	1.277±0.003	1.227±0.003	1.184±0.004	1.170±0.003
SPVI	Pl	137.643±0.525	122.228±0.627	69.423±0.374	130.205±0.287	271.346±1.373
	Ps	125.854±0.901	106.631±0.535	70.051±0.396	126.554±0.407	197.714±4.423
	Sa	118.960±0.959	129.607±0.971	55.994±0.451	130.282±0.352	48.637±0.237
SR	Pl	9.850±0.065	9.464±0.072	7.149±0.065	7.674±0.047	6.562±0.033
	Ps	8.601±0.070	9.085±0.097	7.466±0.060	5.830±0.057	7.254±0.080
	Sa	8.930±0.110	10.133±0.127	7.811±0.108	5.973±0.071	5.334±0.061
SR1	Pl	3.198±0.014	3.245±0.017	2.847±0.013	2.443±0.009	1.956±0.008
	Ps	2.929±0.019	2.737±0.014	2.755±0.016	2.155±0.013	2.187±0.016
	Sa	2.562±0.023	2.876±0.025	2.416±0.021	2.009±0.014	1.863±0.013
SR2	Pl	5.745±0.034	5.626±0.036	4.583±0.029	3.998±0.019	3.227±0.016
	Ps	5.039±0.038	4.693±0.033	4.548±0.033	3.275±0.026	3.526±0.036
	Sa	4.571±0.054	5.193±0.057	4.090±0.048	3.093±0.030	2.856±0.027
SR3	Pl	5.743±0.023	5.614±0.029	4.895±0.028	5.115±0.024	3.914±0.017
	Ps	5.161±0.032	5.092±0.033	4.775±0.030	4.430±0.036	5.466±0.036
	Sa	3.948±0.040	4.652±0.051	3.858±0.044	3.775±0.037	3.093±0.032
SR4	Pl	3.426±0.014	3.153±0.014	2.695±0.023	4.365±0.026	3.965±0.018
	Ps	3.314±0.032	4.189±0.051	2.969±0.021	3.674±0.035	4.387±0.041
	Sa	4.492±0.032	4.308±0.032	4.249±0.042	4.516±0.034	4.488±0.032
SR5	Pl	0.313±0.001	0.336±0.001	0.403±0.003	0.270±0.001	0.281±0.001
	Ps	0.331±0.003	0.290±0.003	0.357±0.003	0.332±0.003	0.268±0.002
	Sa	0.246±0.002	0.257±0.002	0.260±0.002	0.284±0.002	0.268±0.002
SR6	Pl	2.022±0.006	2.068±0.008	1.910±0.007	1.669±0.004	1.420±0.003
	Ps	1.916±0.009	1.833±0.006	1.847±0.008	1.571±0.006	1.571±0.007
	Sa	1.736±0.011	1.885±0.011	1.691±0.010	1.501±0.007	1.422±0.006
SR8	Pl	0.667±0.001	0.650±0.001	0.693±0.003	0.679±0.002	0.621±0.001
	Ps	0.691±0.003	0.650±0.002	0.671±0.002	0.693±0.002	0.621±0.002
	Sa	0.580±0.002	0.585±0.002	0.584±0.002	0.626±0.001	0.609±0.001
Sum_Dr1	Pl	101.645±0.390	88.678±0.445	50.401±0.271	97.595±0.242	207.790±1.106
	Ps	94.157±0.642	80.324±0.402	51.567±0.311	96.257±0.388	144.699±3.283
	Sa	99.467±0.756	104.628±0.792	46.834±0.413	109.850±0.432	48.089±0.341
Sum_Dr2	Pl	95.079±0.359	82.109±0.409	46.761±0.255	87.601±0.207	179.565±0.809
	Ps	87.069±0.617	73.951±0.365	47.867±0.289	84.187±0.337	125.297±2.785
	Sa	88.211±0.673	92.771±0.678	40.920±0.345	88.702±0.237	37.263±0.185
TCARI	Pl	38.057±0.266	34.477±0.336	21.632±0.219	36.069±0.381	102.864±0.787
	Ps	37.974±0.338	31.090±0.467	23.293±0.242	47.506±0.633	39.656±1.145
	Sa	51.123±0.710	48.220±0.776	26.467±0.474	62.481±1.097	35.853±0.579
TCARI/OSAVI	Pl	39.614±0.314	36.565±0.396	24.588±0.296	36.974±0.431	111.322±0.955
	Ps	40.574±0.384	33.561±0.584	25.753±0.289	54.838±0.818	41.927±1.276
	Sa	52.762±0.815	49.199±0.860	28.472±0.573	72.153±1.525	40.272±0.739
TCARI2	Pl	54.822±0.315	48.009±0.406	30.633±0.253	49.658±0.176	79.872±0.475
	Ps	52.009±0.396	45.204±0.339	30.192±0.222	47.247±0.344	50.860±0.761
	Sa	56.750±0.471	56.961±0.569	26.195±0.241	47.851±0.308	20.300±0.180
TCARI2/OSAVI2	Pl	113.949±0.940	100.497±1.163	69.778±0.718	132.696±0.684	290.445±1.057
	Ps	117.351±1.057	108.761±1.117	71.191±0.698	146.208±1.076	172.332±3.683
	Sa	147.954±1.820	140.434±1.996	74.730±1.103	168.498±1.155	86.137±0.819
TGI	Pl	773.435±5.013	727.459±6.576	411.594±3.437	902.592±6.877	2595.189±21.098
	Ps	761.591±11.380	760.911±8.172	470.521±6.064	998.433±13.188	780.819±11.298
	Sa	1467.432±20.288	1410.123±20.658	774.125±13.578	1853.143±25.865	1086.649±14.133
TVI	Pl	5788.733±23.340	4960.724±26.027	2837.263±16.193	5618.543±15.873	11100.485±37.253
	Ps	5333.026±38.153	4677.479±24.468	2929.172±19.779	5441.825±26.989	7249.062±146.671
	Sa	5951.852±48.006	6095.233±47.727	2772.575±26.454	6277.591±23.571	2864.020±19.522
Vogelmann	Pl	1.354±0.002	1.361±0.002	1.335±0.002	1.239±0.001	1.104±0.001
	Ps	1.327±0.003	1.303±0.002	1.307±0.003	1.232±0.002	1.209±0.002
	Sa	1.269±0.004	1.308±0.004	1.260±0.003	1.215±0.002	1.156±0.002

Number of experiment		1	2	3	4	5
VI	Species	Mean of VI value ± SD				
Vogelmann2	Pl	-0.064±0.000	-0.069±0.001	-0.065±0.001	-0.046±0.000	-0.064±0.000
	Ps	-0.057±0.001	-0.055±0.000	-0.056±0.001	-0.040±0.000	-0.060±0.001
	Sa	-0.046±0.001	-0.058±0.001	-0.045±0.001	-0.036±0.000	-0.022±0.001
Vogelmann3	Pl	1.122±0.003	1.188±0.004	1.068±0.005	0.919±0.003	0.659±0.007
	Ps	1.081±0.006	1.041±0.004	1.054±0.004	0.860±0.004	0.746±0.010
	Sa	0.992±0.006	1.076±0.006	0.967±0.006	0.781±0.005	0.901±0.004
Vogelmann4	Pl	-0.069±0.001	-0.075±0.001	-0.070±0.001	-0.048±0.000	-0.065±0.000
	Ps	-0.061±0.001	-0.059±0.001	-0.060±0.001	-0.042±0.000	-0.062±0.001
	Sa	-0.049±0.001	-0.063±0.001	-0.048±0.001	-0.038±0.000	-0.023±0.001

Notes: Orange color indicates the values for which $p > 0.05$ (Wilcox Test)

Table 6
Number of the vegetation indices significantly differing between the compared *Acer* species pairs according to the Wilcox Test.

Species	*A. saccharinum*	*A. platanoides*	*A. pseudoplatanus*
A.saccharinum	0	68	63
A. platanoides	68	0	56
A. pseudoplatanus	63	56	0

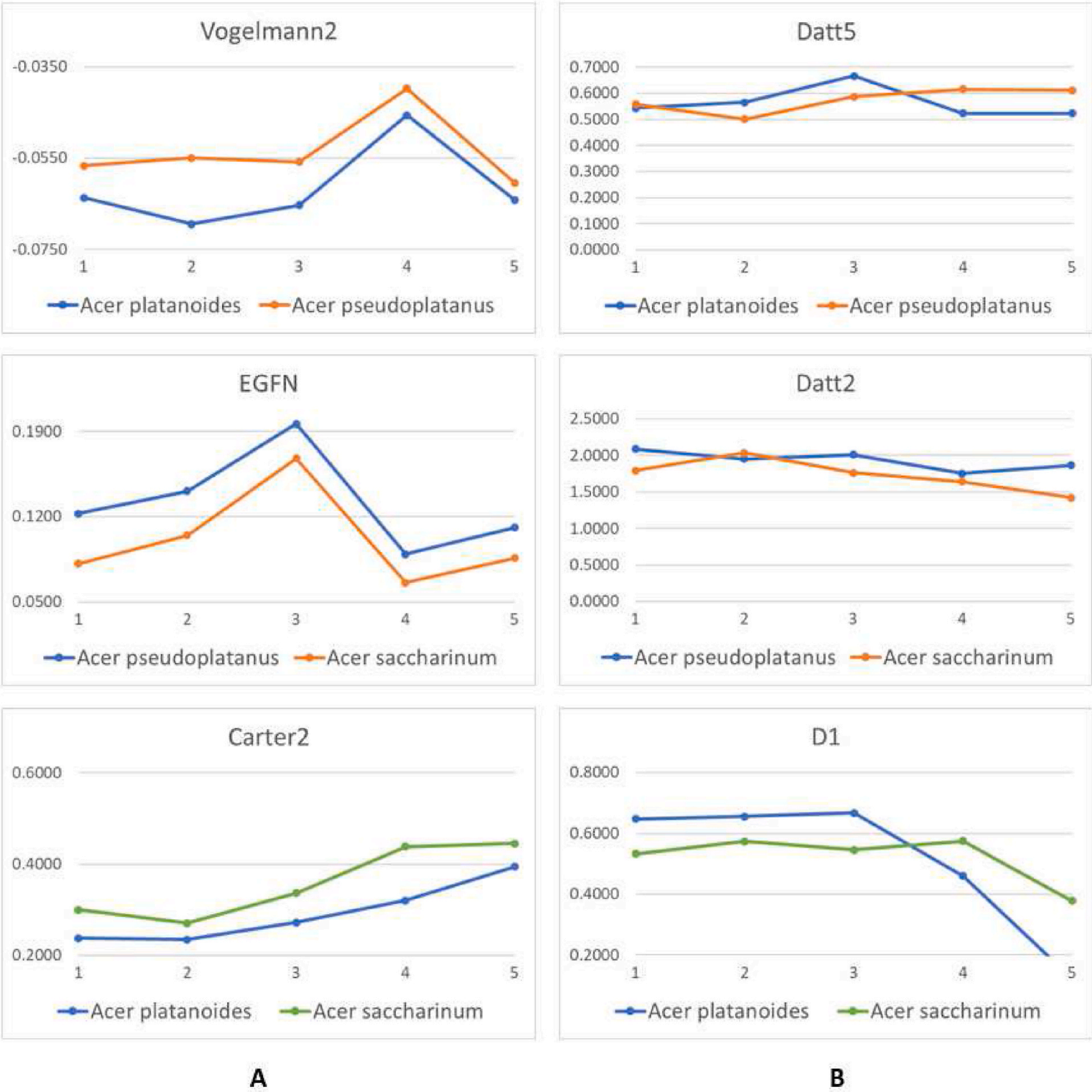

Fig. 5. Dynamics of changes in the values of vegetation indices during the five experiments. A - kept the trend in all experiments; B - did not save the unidirectional trend.
Notes: For all the compared *Acer* pairs shown in the figure, the values of the vegetation indices during the five experiments significantly differ according to the Wilcox Test at a confidence level of 0.95 (Table 5).

Table 7
Vegetation indexes suitable to distinguish *Acer* species.

Compared species	Vegetation indexes
A. platanoides vs A. pseudoplatanus	Boochs2, MCARI2, TCARI2, Vogelmann2, Vogelmann4
A. platanoides vs A. saccharinum	Carter2, Carter3, Carter4, Carter5, CI, CI2, CRI3, CRI4, Datt, Datt2, Datt3, Datt5, DDn, DWSI4, EGFN, EGFR, EVI, GI, GMI1, GMI2, Green NDVI, Maccioni, MCARI2, mSR2, MTCI, NDVI2, NDVI3, OSAVI2, PARS, PSSR, REP_Li, SR1, SR2, SR3, SR4, SR8, Vogelmann2, Vogelmann4
A. pseudoplatanus vs A. saccharinum	Carter3, Carter5, CRI3, Datt5, Datt6, DWSI4, EGFN, EGFR, GI, GMI1, Green NDVI, NDVI3, PARS, SR3, SR4, SR5, SR8, TGI

Table 8
Channels used for calculating vegetation indexes suitable to distinguish *Acer* species.

Wavelength	474	478	482	486	490	494	498	502	506	510	514	518	522	526	530	538	542	546	550	554	558	562	566	570
Spectral channel	7	8	9	10	11	12	13	14	15	16	17	18	19	20	21	22	23	24	25	26	27	28	29	30
A. platanoides vs A. pseudoplatanus							x																	
A. platanoides vs A. saccharinum	x									x	x								x	x				
A. pseudoplatanus vs A. saccharinum		x								x	x								x	x				

Wavelength	574	578	582	586	590	594	598	602	606	610	614	618	622	626	630	634	638	642	646	650	654	658	662	666
Spectral channel	31	32	33	34	35	36	37	38	39	40	41	42	43	44	45	46	47	48	49	50	51	52	53	54
A. platanoides vs A. pseudoplatanus																								
A. platanoides vs A. saccharinum								x								x						x		x
A. pseudoplatanus vs A. saccharinum								x																

Wavelength	670	674	678	682	686	690	694	698	702	706	710	714	718	722	726	730	734	738	742	746	750	754	758	762
Spectral channel	55	56	57	58	59	60	61	62	63	64	65	66	67	68	69	70	71	72	73	74	75	76	77	78
A. platanoides vs A. pseudoplatanus	x							x	x			x	x		x		x			x	x			
A. platanoides vs A. saccharinum	x	x	x	x		x	x	x	x	x	x	x	x		x		x	x		x	x	x	x	
A. pseudoplatanus vs A. saccharinum	x	x	x	x			x	x		x										x	x		x	

Wavelength	766	770	774	778	782	786	790	794	798	802	806	810	814	818	822	826	830	834	838	842	846	850	854	858
Spectral channel	79	80	81	82	83	84	85	86	87	88	89	90	91	92	93	94	95	96	97	98	99	100	101	102
A. platanoides vs A. pseudoplatanus																								
A. platanoides vs A. saccharinum		x		x					x													x		
A. pseudoplatanus vs A. saccharinum		x							x															x

Notes: Channels used for calculating vegetation indices for all 3 pairs of *Acer* are marked in green

operational inventory of green spaces and for remote sensing base monitoring and classification of tree speices.

Ethics approval and consent to participate

Not applicable.

Consent for publication

Not applicable.

Availability of data and material

All data generated or analyzed during this study are included in this manuscript.

Conflicts of interest

The authors declare that they have no competing interests.

Funding

The research was financially supported by the Ministry of Science and Higher Education of the Russian Federation within the framework of the state task in the field of scientific activity (no. 0852-2020-0029).

Ethical statement

Authors have followed all the ethics of research in this manuscript.

CRediT authorship contribution statement

Pavel A. Dmitriev: Conceptualization, made the concept, experiment planning, Data curation, Formal analysis, Writing – original draft, prepare the original draft, prepare the figures and prepare the final draft, All authors read and approved the final manuscript. **Boris L. Kozlovsky:** Conceptualization, made the concept, experiment planning, Data curation, Formal analysis, All authors read and approved the final manuscript. **Denis P. Kupriushkin:** Conceptualization, made the concept, experiment planning, Data curation, Formal analysis, All authors read and approved the final manuscript. **Vladimir S. Lysenko:** Conceptualization, made the concept, experiment planning, Data curation, Formal analysis, All authors read and approved the final manuscript. **Vishnu D. Rajput:** Conceptualization, made the concept, experiment planning, Data curation, Formal analysis, All authors read and approved the final manuscript. **Maria A. Ignatova:** Conceptualization, made the concept, experiment planning, Data curation, Formal analysis, All authors read and approved the final manuscript. **Olga A. Kapralova:** Conceptualization, made the concept, experiment planning, Data curation, Formal analysis, Writing – original draft, prepare the original draft, All authors read and approved the final manuscript. **Valeriy K. Tokhtar:** Conceptualization, made the concept, experiment planning, Data curation, Formal analysis, Writing – original draft, prepare the original draft, All authors read and approved the final manuscript. **Anil Kumar Singh:** Writing – review & editing, made the review and editing, All authors read and approved the final manuscript. **Tatiana Minkina:** Writing – review & editing, made the review and editing, All authors read and approved the final manuscript. **Tatiana V. Varduni:** Writing – review & editing, made the review and editing, prepare the figures and prepare the final draft. All authors read and approved the final manuscript. **Meenakshi Sharma:** prepare the figures and prepare the final draft. All authors read and approved the final manuscript. **Ajay Kumar Taloor:** Writing – review & editing, made the review and editing, prepare the figures and prepare the final draft. All authors read and approved the final manuscript. **Asha Thapliyal:** prepare the figures and prepare the final draft. All authors read and approved the final manuscript.

Declaration of competing interest

The authors declare that they have no known competing financial interests or personal relationships that could have appeared to influence the work reported in this paper.

Acknowledgements

The research was performed with the equipment of Multiaccess Center 'Biotechnology, biomedicine and environmental monitoring' and Multiaccess Center 'High technologies' of Southern Federal University (Rostov-on-Don).

Appendix A. Supplementary data

Supplementary data to this article can be found online at https://doi.org/10.1016/j.rsase.2021.100679.

References

Aasen, H., Bolten, A., 2018. Multi-temporal high-resolution imaging spectroscopy with hyperspectral 2D imagers – from theory to application. Remote Sens. Environ. 205, 374–389. https://doi.org/10.1016/J.RSE.2017.10.043.

Aasen, H., Burkart, A., Bolten, A., Bareth, G., Aasen, H., Burkart, A., Bolten, A., Bareth, G., 2015. Generating 3D hyperspectral information with lightweight UAV snapshot cameras for vegetation monitoring: from camera calibration to quality assurance. JPRS 108, 245–259. https://doi.org/10.1016/J.ISPRSJPRS.2015.08.002.

Adão, T., Hruška, J., Pádua, L., Bessa, J., Peres, E., Morais, R., Sousa, J.J., 2017. Hyperspectral imaging: a review on UAV-based sensors, data processing and applications for agriculture and forestry. Rem. Sens. 9 https://doi.org/10.3390/RS9111110.

Akhtman, Y., Golubeva, E.I., Tutubalina, O.V., Zimin, M., 2017. Application of hyperspectural images and ground data for precision farming. Geogr. Environ. Sustain. 10, 117–128. https://doi.org/10.24057/2071-9388-2017-10-4-117-128.

Antonucci, F., Menesatti, P., Holden, N.M., Canali, E., Giorgi, S., Maienza, A., Stazi, S.R., 2012. Hyperspectral visible and near-infrared determination of copper concentration in agricultural polluted soils. Commun. Soil Sci. Plant Anal. 43, 1401–1411. https://doi.org/10.1080/00103624.2012.670348.

Apan, A., Held, A., Phinn, S.R., Markley, J., 2004. Detecting sugarcane "orange rust" disease using EO-1 Hyperion hyperspectral imagery. Int. J. Rem. Sens. 25, 489–498. https://doi.org/10.1080/01431160310001618031.

R, H.-C., Rm, N.-C., Pj, Z.-T., 2012. Carotenoid content estimation in a heterogeneous conifer forest using narrow-band indices and PROSPECT+DART simulations. Remote Sens. Environ. 127, 298–315. https://doi.org/10.1016/J.RSE.2012.09.014.

Bannari, A., Staenz, K., Champagne, C., Khurshid, K.S., 2015. Spatial variability mapping of crop residue using hyperion (EO-1) hyperspectral data. Rem. Sens. 7, 8107–8127. https://doi.org/10.3390/RS70608107.

Bareth, G., Aasen, H., Bendig, J., Gnyp, M.L., Bolten, A., Jung, A., Michels, R., Soukkamäki, J., 2015. Low-weight and UAV-based hyperspectral full-frame cameras for monitoring crops: spectral comparison with portable spectroradiometer measurements. Photogramm. Fernerkund. GeoInf. 69–79. https://doi.org/10.1127/PFG/2015/0256, 2015.

Behmann, J., Mahlein, A.-K., Paulus, S., Kuhlmann, H., Oerke, E.-C., Plümer, L., 2014. Generation and application of hyperspectral 3D plant models. Lect. Notes Comput. Sci. (including Subser. Lect. Notes Artif. Intell. Lect. Notes Bioinformatics) 8928, 117–130. https://doi.org/10.1007/978-3-319-16220-1_9.

Blackburn, G.A., 1998. Quantifying chlorophylls and caroteniods at leaf and canopy scales: an evaluation of some hyperspectral approaches. Remote Sens. Environ. 66, 273–285. https://doi.org/10.1016/S0034-4257(98)00059-5.

Broge, N.H., Leblanc, E., 2001. Comparing prediction power and stability of broadband and hyperspectral vegetation indices for estimation of green leaf area index and canopy chlorophyll density. Remote Sens. Environ. 76, 156–172. https://doi.org/10.1016/S0034-4257(00)00197-8.
Camacho Velasco, A., Vargas García, C.A., Arguello Fuentes, H., 2016. A comparative study of target detection algorithms in hyperspectral imagery applied to agricultural crops in Colombia. Tecnura 20, 86–99. https://doi.org/10.14483/UDISTRITAL.JOUR.TECNURA.2016.3.A06.
Chappelle, E.W., Kim, M.S., McMurtrey, J.E., 1992. Ratio analysis of reflectance spectra (RARS): an algorithm for the remote estimation of the concentrations of chlorophyll A, chlorophyll B, and carotenoids in soybean leaves. Remote Sens. Environ. 39, 239–247. https://doi.org/10.1016/0034-4257(92)90089-3.
Chen, J.M., 1996. Evaluation of vegetation indices and a modified simple ratio for boreal applications. Can. J. Rem. Sens. 22, 229–242. https://doi.org/10.1080/07038992.1996.10855178.
Dash, J., Curran, P.J., 2004. The MERIS terrestrial chlorophyll index. Int. J. Rem. Sens. 25, 5403–5413. https://doi.org/10.1080/0143116042000274015.
Datt, B., 1998. Remote sensing of chlorophyll a, chlorophyll b, chlorophyll a+b, and total carotenoid content in Eucalyptus leaves. Remote Sens. Environ. 66, 111–121. https://doi.org/10.1016/S0034-4257(98)00046-7.
Datt, B., 1999. Visible/near infrared reflectance and chlorophyll content in eucalyptus leaves. Int. J. Rem. Sens. 20, 2741–2759. https://doi.org/10.1080/014311699211778.
Daughtry, C.S.T., Walthall, C.L., Kim, M.S., De Colstoun, E.B., McMurtrey, J.E., 2000. Estimating corn leaf chlorophyll concentration from leaf and canopy reflectance. Remote Sens. Environ. 74, 229–239. https://doi.org/10.1016/S0034-4257(00)00113-9.
Dutta, S., Bhattacharya, B.K., Rajak, D.R., Chattopadhayay, C., Patel, N.K., Parihar, J.S., 2006. Disease detection in mustard crop using eo-1 hyperion satellite data. J. Indian Soc. Remote Sens. 343 34, 325–330. https://doi.org/10.1007/BF02990661, 2006.
Eddy, P.R., Smith, A.M., Hill, B.D., Peddle, D.R., Coburn, C.A., Blackshaw, R.E., 2008. Hybrid segmentation - artificial neural network classification of high resolution hyperspectral imagery for site-specific herbicide management in agriculture. Photogramm. Eng. Rem. Sens. 74, 1249–1257. https://doi.org/10.14358/PERS.74.10.1249.
Elvidge, C.D., Chen, Z., 1995. Comparison of broad-band and narrow-band red and near-infrared vegetation indices. Remote Sens. Environ. 54, 38–48. https://doi.org/10.1016/0034-4257(95)00132-K.
Estep, L., Terrie, G., Davis, B., 2004. Crop stress detection using AVIRIS hyperspectral imagery and artificial neural networks. Int. J. Rem. Sens. 25, 4999–5004. https://doi.org/10.1080/01431160412331291242.
Fassnacht, F.E., Neumann, C., Forster, M., Buddenbaum, H., Ghosh, A., Clasen, A., Joshi, P.K., Koch, B., 2014. Comparison of feature reduction algorithms for classifying tree species with hyperspectral data on three central european test sites. IEEE J. Sel. Top. Appl. Earth Obs. Rem. Sens. 7, 2547–2561. https://doi.org/10.1109/JSTARS.2014.2329390.
Fassnacht, F.E., Latifi, H., Stereńczak, K., Modzelewska, A., Lefsky, M., Waser, L.T., Straub, C., Ghosh, A., 2016. Review of studies on tree species classification from remotely sensed data. Remote Sens. Environ. 186, 64–87. https://doi.org/10.1016/J.RSE.2016.08.013.
Feng, H., Chen, G., Xiong, L., Liu, Q., Yang, W., 2017. Accurate digitization of the chlorophyll distribution of individual rice leaves using hyperspectral imaging and an integrated image analysis pipeline. Front. Plant Sci. 8 https://doi.org/10.3389/FPLS.2017.01238/FULL.
Fenghua, Y., Tongyu, X., Wen, D., Hang, M., Guosheng, Z., Chunling, C., 2017. Radiative transfer models (RTMs) for field phenotyping inversion of rice based on UAV hyperspectral remote sensing. Int. J. Agric. Biol. Eng. 10, 150–157. https://doi.org/10.25165/IJABE.V10I4.3076.
Filella, I., Peñuelas, J., 1994. The red edge position and shape as indicators of plant chlorophyll content, biomass and hydric status. Int. J. Rem. Sens. 15, 1459–1470. https://doi.org/10.1080/01431169408954177.
Fricker, G.A., Ventura, J.D., Wolf, J.A., North, M.P., Davis, F.W., Franklin, J., Fricker, G.A., Ventura, J.D., Wolf, J.A., North, M.P., Davis, F.W., Franklin, J., 2019. A convolutional neural network classifier identifies tree species in mixed-conifer forest from hyperspectral imagery. RemS 11, 2326. https://doi.org/10.3390/RS11192326.
Galloza, M.S., Crawford, M., 2011. Exploiting multisensor spectral data to improve crop residue cover estimates for management of agricultural water quality. Int. Geosci. Remote Sens. Symp. 3668–3671. https://doi.org/10.1109/IGARSS.2011.6050020.
S.Gandia , G. Fernandez G, J. Garcia, M., 2004. RETRIEVAL OF VEGETATION BIOPHYSICAL VARIABLES FROM CHRIS/PROBA DATA IN THE SPARC CAMPAING. ESA SP 578, 40-48.
Garrity, S.R., Eitel, J.U.H., Vierling, L.A., 2011. Disentangling the relationships between plant pigments and the photochemical reflectance index reveals a new approach for remote estimation of carotenoid content. Remote Sens. Environ. 115, 628–635. https://doi.org/10.1016/J.RSE.2010.10.007.
Gitelson, A., Merzlyak, M.N., 1994. Quantitative estimation of chlorophyll-a using reflectance spectra: experiments with autumn chestnut and maple leaves. J. Photochem. Photobiol. B Biol. 22, 247–252. https://doi.org/10.1016/1011-1344(93)06963-4.
Gitelson, A.A., Merzlyak, M.N., 1997. Remote estimation of chlorophyll content in higher plant leaves. Int. J. Rem. Sens. 18, 2691–2697. https://doi.org/10.1080/014311697217558.
Gitelson, A.A., Kaufman, Y.J., Merzlyak, M.N., 1996. Use of a green channel in remote sensing of global vegetation from EOS-MODIS. Remote Sens. Environ. 58, 289–298. https://doi.org/10.1016/S0034-4257(96)00072-7.
Gitelson, A.A., Buschmann, C., Lichtenthaler, H.K., 1999. The chlorophyll fluorescence ratio F735F700 as an accurate measure of the chlorophyll content in plants. Remote Sens. Environ. 69, 296–302. https://doi.org/10.1016/S0034-4257(99)00023-1.
Gitelson, A.A., Gritz, Y., Merzlyak, M.N., 2003. Relationships between leaf chlorophyll content and spectral reflectance and algorithms for non-destructive chlorophyll assessment in higher plant leaves. J. Plant Physiol. 160, 271–282. https://doi.org/10.1078/0176-1617-00887.
Glenn, N.F., Mitchell, J.J., Anderson, M.O., Hruska, R.C., 2012. UNMANNED AERIAL VEHICLE (UAV) HYPERSPECTRAL REMOTE SENSING for DRYLAND VEGETATION MONITORING. Hyperspectral Image Signal Process. Evol. Remote Sensing,Shanghai, China,06/04/2012,06/07/2012.
Goel, P.K., Prasher, S.O., Landry, J.-A., Patel, R.M., Viau, A.A., 2003. Hyperspectral image classification to detect weed infestations and nitrogen status IN corn. Trans. ASAE (American Soc. Agric. Eng. 46, 539–550.
Goetz, A.F.H., 2009. Three decades of hyperspectral remote sensing of the Earth: a personal view. Remote Sens. Environ. 113, S5–S16. https://doi.org/10.1016/J.RSE.2007.12.014.
Gomez, C., Viscarra Rossel, R.A., McBratney, A.B., 2008. Soil organic carbon prediction by hyperspectral remote sensing and field vis-NIR spectroscopy: an Australian case study. Geoderma 146, 403–411. https://doi.org/10.1016/J.GEODERMA.2008.06.011.
Gonzalez-Dugo, V., Hernandez, P., Solis, I., Zarco-Tejada, P.J., 2015. Using high-resolution hyperspectral and thermal airborne imagery to assess physiological condition in the context of wheat phenotyping. Rem. Sens. 7, 13586–13605. https://doi.org/10.3390/RS71013586.
Guyot, G., Baret, F., 1988. Utilisation de la Haute Resolution Spectrale pour Suivre L'etat des Couverts Vegetaux. ESASP 287, 279.
Haboudane, D., Miller, J.R., Tremblay, N., Zarco-Tejada, P.J., Dextraze, L., 2002. Integrated narrow-band vegetation indices for prediction of crop chlorophyll content for application to precision agriculture. Remote Sens. Environ. 81, 416–426. https://doi.org/10.1016/S0034-4257(02)00018-4.
Hernández-Clemente, R., Navarro-Cerrillo, R.M., Suárez, L., Morales, F., Zarco-Tejada, P.J., 2011. Assessing structural effects on PRI for stress detection in conifer forests. Remote Sens. Environ. 115, 2360–2375. https://doi.org/10.1016/J.RSE.2011.04.036.
Honkavaara, E., Kaivosoja, J., Mäkynen, J., Pellikka, I., Pesonen, L., Saari, H., Salo, H., Hakala, T., Marklelin, L., Rosnell, T., 2012. Hyperspectral reflectance signatures and point clouds for precision agriculture by light weight Uav imaging system. ISPAn I7, 353–358. https://doi.org/10.5194/ISPRSANNALS-I-7-353-2012.
Houborg, R., Fisher, J.B., Skidmore, A.K., 2015. Advances in remote sensing of vegetation function and traits. Int. J. Appl. Earth Obs. Geoinf. 43, 1–6. https://doi.org/10.1016/J.JAG.2015.06.001.
Hruska, R., Mitchell, J., Anderson, M., Glenn, N.F., 2012. Radiometric and geometric analysis of hyperspectral imagery acquired from an unmanned aerial vehicle. Rem. Sens. 4, 2736–2752. https://doi.org/10.3390/RS4092736.
Huete, A.R., 1988. A soil-adjusted vegetation index (SAVI). Remote Sens. Environ. 25, 295–309. https://doi.org/10.1016/0034-4257(88)90106-X.
Huete, A.R., Liu, H.Q., Batchily, K., Van Leeuwen, W., 1997. A comparison of vegetation indices over a global set of TM images for EOS-MODIS. Remote Sens. Environ. 59, 440–451. https://doi.org/10.1016/S0034-4257(96)00112-5.

Hunt, E., Doraiswamy, P., McMurtrey, J., Daughtry, C., Perry, E., Akhmedov, B., 2013. A Visible Band Index for Remote Sensing Leaf Chlorophyll Content at the Canopy Scale. Publ. from USDA-ARS/UNL Fac.

Hycza, T., Stereńczak, K., Bałazy, R., 2018. Potential use of hyperspectral data to classify forest tree species. New Zeal. J. For. Sci. 481 48, 1–13. https://doi.org/10.1186/S40490-018-0123-9, 2018.

Izzo, R.R., Lakso, A.N., Marcellus, E.D., Bauch, T.D., Raqueño, N.G., Aardt, J. van, 2019. An initial analysis of real-time sUAS-based detection of grapevine water status in the Finger Lakes wine country of upstate. N. Y. 11008, 1100811. https://doi.org/10.1117/12.2518762.

Jordan, C.F., 1969. Derivation of leaf-area index from quality of light on the forest floor. Ecology 50, 663–666. https://doi.org/10.2307/1936256.

Kaivosoja, J., Pesonen, L., Kleemola, J., Pölönen, I., Salo, H., Honkavaara, E., Saari, H., Mäkynen, J., Rajala, A., 2013. A case study of a precision fertilizer application task generation for wheat based on classified hyperspectral data from UAV combined with farm history data. Remote Sens. Agric. Ecosyst. Hydrol. XV 8887, 88870H. https://doi.org/10.1117/12.2029165.

Kim, M.S., Daughtry, C., Chappelle, E., McMurtrey, J., Walthall, C., 1994. The Use of High Spectral Resolution Bands for Estimating Absorbed Photosynthetically Active Radiation (A Par). Undefined.

Lehnert, L.W., Meyer, H., Obermeier, W.A., Silva, B., Regeling, B., Thies, B., Bendix, J., 2019. Hyperspectral data analysis in R: the hsdar package. J. Stat. Software 89 (12), 1–23. https://doi.org/10.18637/jss.v089.i12.

Liu, J., Miller, J.R., Haboudane, D., Pattey, E., Hochheim, K., 2008. Crop fraction estimation from casi hyperspectral data using linear spectral unmixing and vegetation indices. Can. J. Rem. Sens. 34, S124–S138. https://doi.org/10.5589/M07-062.

Lopatin, J., Fassnacht, F.E., Kattenborn, T., Schmidtlein, S., 2017. Mapping plant species in mixed grassland communities using close range imaging spectroscopy. Remote Sens. Environ. 201, 12–23. https://doi.org/10.1016/J.RSE.2017.08.031.

Lu, B., Dao, P.D., Liu, J., He, Y., Shang, J., 2020. Recent advances of hyperspectral imaging technology and applications in agriculture, 2020 Rem. Sens. 12, 2659. https://doi.org/10.3390/RS12162659, 2659 12.

Lucieer, A., Malenovský, Z., Veness, T., Wallace, L., 2014. HyperUAS—imaging spectroscopy from a multirotor unmanned aircraft system. J. Field Robot. 31, 571–590. https://doi.org/10.1002/ROB.21508.

Maccioni, A., Agati, G., Mazzinghi, P., 2001. New vegetation indices for remote measurement of chlorophylls based on leaf directional reflectance spectra. J. Photochem. Photobiol. B Biol. 61, 52–61. https://doi.org/10.1016/S1011-1344(01)00145-2.

Malmir, M., Tahmasbian, I., Xu, Z., Farrar, M.B., Bai, S.H., 2019. Prediction of soil macro- and micro-elements in sieved and ground air-dried soils using laboratory-based hyperspectral imaging technique. Geoderma 340, 70–80. https://doi.org/10.1016/J.GEODERMA.2018.12.049.

Mäyrä, J., Keski-Saari, S., Kivinen, S., Tanhuanpää, T., Hurskainen, P., Kullberg, P., Poikolainen, L., Viinikka, A., Tuominen, S., Kumpula, T., Vihervaara, P., 2021. Tree species classification from airborne hyperspectral and LiDAR data using 3D convolutional neural networks. Remote Sens. Environ. 256, 112322. https://doi.org/10.1016/J.RSE.2021.112322.

McMurtrey, J.E., Chappelle, E.W., Kim, M.S., Meisinger, J.J., Corp, L.A., 1994. Distinguishing nitrogen fertilization levels in field corn (Zea mays L.) with actively induced fluorescence and passive reflectance measurements. Remote Sens. Environ. 47, 36–44. https://doi.org/10.1016/0034-4257(94)90125-2.

Merzlyak, M.N., Gitelson, A.A., Chivkunova, O.B., Rakitin, V.Y., 1999. Non-destructive optical detection of pigment changes during leaf senescence and fruit ripening. Physiol. Plantarum 106, 135–141. https://doi.org/10.1034/J.1399-3054.1999.106119.X.

Moharana, S., Dutta, S., 2016. Spatial variability of chlorophyll and nitrogen content of rice from hyperspectral imagery. ISPRS J. Photogrammetry Remote Sens. 122, 17–29. https://doi.org/10.1016/J.ISPRSJPRS.2016.09.002.

Mohd Asaari, M.S., Mishra, P., Mertens, S., Dhondt, S., Inzé, D., Wuyts, N., Scheunders, P., 2018. Close-range hyperspectral image analysis for the early detection of stress responses in individual plants in a high-throughput phenotyping platform. ISPRS J. Photogrammetry Remote Sens. 138, 121–138. https://doi.org/10.1016/J.ISPRSJPRS.2018.02.003.

Morel, J., Jay, S., Feret, J.B., Bakache, A., Bendoula, R., Carreel, F., Gorretta, N., 2018. Exploring the potential of PROCOSINE and close-range hyperspectral imaging to study the effects of fungal diseases on leaf physiology. Sci. Rep. 8 https://doi.org/10.1038/S41598-018-34429-0.

Nagasubramanian, K., Jones, S., Singh, A.K., Sarkar, S., Singh, A., Ganapathysubramanian, B., 2019. Plant disease identification using explainable 3D deep learning on hyperspectral images. Plant Methods 151 15, 1–10. https://doi.org/10.1186/S13007-019-0479-8, 2019.

Nigam, R., Tripathy, R., Dutta, S., Bhagia, N., Nagori, R., Chandrasekar, K., Kot, R., Bhattacharya, B.K., Ustin, S., 2019. Crop type discrimination and health assessment using hyperspectral imaging. Curr. Sci. 116, 1108–1123. https://doi.org/10.18520/CS/V116/I7/1108-1123.

Oppelt, N., Mauser, W., 2004. Hyperspectral monitoring of physiological parameters of wheat during a vegetation period using AVIS data. Int. J. Rem. Sens. 25, 145–159. https://doi.org/10.1080/0143116031000115300.

Palacios-Orueta, A., Ustin, S.L., 1998. Remote sensing of soil properties in the Santa Monica Mountains I. Spectral analysis. Remote Sens. Environ. 65, 170–183. https://doi.org/10.1016/S0034-4257(98)00024-8.

Peñuelas, J., Gamon, J.A., Fredeen, A.L., Merino, J., Field, C.B., 1994. Reflectance indices associated with physiological changes in nitrogen- and water-limited sunflower leaves. Remote Sens. Environ. 48, 135–146. https://doi.org/10.1016/0034-4257(94)90136-8.

Pölönen, I., Saari, H., Kaivosoja, J., Honkavaara, E., Pesonen, L., 2013. Hyperspectral imaging based biomass and nitrogen content estimations from light-weight UAV. Remote Sens. Agric. Ecosyst. Hydrol. XV 8887, 88870J. https://doi.org/10.1117/12.2028624.

Qi, J., Chehbouni, A., Huete, A.R., Kerr, Y.H., Sorooshian, S., 1994. A modified soil adjusted vegetation index. Remote Sens. Environ. 48, 119–126. https://doi.org/10.1016/0034-4257(94)90134-1.

Ran, Q., Li, W., Du, Q., Yang, C., 2015. Hyperspectral image classification for mapping agricultural tillage practices. J. Appl. Remote Sens. 9, 097298 https://doi.org/10.1117/1.JRS.9.097298.

Rondeaux, G., Steven, M., Baret, F., 1996. Optimization of soil-adjusted vegetation indices. Remote Sens. Environ. 55, 95–107. https://doi.org/10.1016/0034-4257(95)00186-7.

Roujean, J.L., Breon, F.M., 1995. Estimating PAR absorbed by vegetation from bidirectional reflectance measurements. Remote Sens. Environ. 51, 375–384. https://doi.org/10.1016/0034-4257(94)00114-3.

Scherrer, B., Sheppard, J., Jha, P., Shaw, J.A., 2019. Hyperspectral imaging and neural networks to classify herbicide-resistant weeds. J. Appl. Remote Sens. 13, 044516 https://doi.org/10.1117/1.JRS.13.044516.

Shivers, S.W., Roberts, D.A., McFadden, J.P., Tague, C., 2018. Using imaging spectrometry to study changes in crop area in California's Central Valley during Drought. Rem. Sens. 10 https://doi.org/10.3390/RS10101556.

Singh, A., Rajput, V., Rawat, S., Singh, A.K., Bind, A., Singh, A.K., Chernikova, N., Voloshina, M., Lobzenko, I., 2020. Monitoring soil salinity and recent advances in mechanism of salinity tolerance in plants. Biogeosystem Tech. 7, 66–87. https://doi.org/10.13187/bgt.2020.2.66.

Smith, R.C.G., Adams, J., Stephens, D.J., Hick, P.T., 1995. Forecasting wheat yield in a Mediterranean-type environment from the NOAA satellite. Aust. J. Agric. Res. 46, 113–125. https://doi.org/10.1071/AR9950113.

Sw, S., Da, R., Jp, M., 2019. Using paired thermal and hyperspectral aerial imagery to quantify land surface temperature variability and assess crop stress within California orchards. Remote Sens. Environ. 222, 215–231. https://doi.org/10.1016/J.RSE.2018.12.030.

Tucker, C.J., 1979. Red and photographic infrared linear combinations for monitoring vegetation. Remote Sens. Environ. 8, 127–150. https://doi.org/10.1016/0034-4257(79)90013-0.

Vincini, M., Frazzi, E., Alessio, P., 2006. Angular dependence of maize and sugar beet VIs from directional CHRIS/PROBA data. Fourth ESA CHRIS PROBA. Work. ESRIN 1, 19–21.

Vogelmann, J.E., Rock, B.N., Moss, D.M., 1993. Red edge spectral measurements from sugar maple leaves. Int. J. Rem. Sens. 14, 1563–1575. https://doi.org/10.1080/01431169308953986.

Wang, T., Liu, Y., Wang, M., Fan, Q., Tian, H., Qiao, X., Li, Y., 2021. Applications of UAS in crop biomass monitoring: a review. Front. Plant Sci. 595. https://doi.org/10.3389/FPLS.2021.616689, 0.

Wolf, F.T., Wolf, F.A., 1955. The carotenoid pigments of the cedar apple rust fungus. Exp 115 11, 179–180. https://doi.org/10.1007/BF02161303, 1955.

Wu, C., Niu, Z., Tang, Q., Huang, W., 2008. Estimating chlorophyll content from hyperspectral vegetation indices: modeling and validation. Agric. For. Meteorol. 148, 1230–1241. https://doi.org/10.1016/J.AGRFORMET.2008.03.005.
Wu, C., Han, X., Niu, Z., Dong, J., 2010. An Evaluation of EO-1 Hyperspectral Hyperion Data for Chlorophyll Content and Leaf Area Index Estimation. https://doi.org/10.1080/01431160903252335, 1079–1086.
Wu, C. Da, McNeely, E., Cedeño-Laurent, J.G., Pan, W.C., Adamkiewicz, G., Dominici, F., Lung, S.C.C., Su, H.J., Spengler, J.D., 2014. Linking student performance in Massachusetts elementary schools with the "greenness" of school surroundings using remote sensing. PLoS One 9. https://doi.org/10.1371/JOURNAL.PONE.0108548.
Xue, J., Su, B., 2017. Significant remote sensing vegetation indices: a review of developments and applications. J. Sensors 2017. https://doi.org/10.1155/2017/1353691.
Yue, J., Yang, G., Li, C., Li, Z., Wang, Y., Feng, H., Xu, B., 2017. Estimation of winter wheat above-ground biomass using unmanned aerial vehicle-based snapshot hyperspectral sensor and crop height improved models. Rem. Sens. 9 https://doi.org/10.3390/RS9070708.
Zarco-Tejada, P.J., Miller, J.R., 1999. Land cover mapping at BOREAS using red edge spectral parameters from CASI imagery. J. Geophys. Res. Atmos. 104, 27921–27933. https://doi.org/10.1029/1999JD900161.
Zarco-Tejada, P.J., Pushnik, J.C., Dobrowski, S., Ustin, S.L., 2003. Steady-state chlorophyll a fluorescence detection from canopy derivative reflectance and double-peak red-edge effects. Remote Sens. Environ. 84, 283–294. https://doi.org/10.1016/S0034-4257(02)00113-X.
Zarco-Tejada, P.J., González-Dugo, V., Williams, L.E., Suárez, L., Berni, J.A.J., Goldhamer, D., Fereres, E., 2013. A PRI-based water stress index combining structural and chlorophyll effects: assessment using diurnal narrow-band airborne imagery and the CWSI thermal index. Remote Sens. Environ. 138, 38–50. https://doi.org/10.1016/J.RSE.2013.07.024.
Zhang, T., Li, L., Zheng, B., 2013. Estimation of agricultural soil properties with imaging and laboratory spectroscopy. JARS 7, 073587. https://doi.org/10.1117/1.JRS.7.073587.
Zhang, C., Walters, D., Kovacs, J.M., 2014. Applications of low altitude remote sensing in agriculture upon farmers' requests-a case study in northeastern Ontario, Canada. PLoS One 9. https://doi.org/10.1371/JOURNAL.PONE.0112894.
Zhu, W., Li, J., Li, L., Wang, A., Wei, X., Mao, H., 2020. Nondestructive diagnostics of soluble sugar, total nitrogen and their ratio of tomato leaves in greenhouse by polarized spectra–hyperspectral data fusion. Int. J. Agric. Biol. Eng. 13, 189–197. https://doi.org/10.25165/IJABE.V13I2.4280.